THESIS FOR THE DEGREE OF LICENTIATE OF ENGINEERING

Development and Characterization of Reliable Graphene-based Materials for Lightweight and Efficient Thermal Management in Electronics

MARKUS ENMARK

Department of Microtechnology and Nanoscience – MC2

CHALMERS UNIVERSITY OF TECHNOLOGY

Gothenburg, Sweden 2024

Development and Characterization of Reliable Graphene-based Materials for Lightweight and Efficient Thermal Management in Electronics
MARKUS ENMARK

ISSN 1652–0769
Technical report no MC2 - 465

Chalmers University of Technology
Department of Microtechnology and Nanoscience – MC2
Electronics Materials and Systems Laboratory
SE-412 96 Göteborg, Sweden
Telephone + 46 (0)31-772 1000

Chalmers digitaltryck
Gothenburg, Sweden 2024

Development and Characterization of Reliable Graphene-based Materials for Lightweight and Efficient Thermal Management in Electronics

MARKUS ENMARK
Department of Microtechnology and Nanoscience – MC2
Chalmers University of Technology

Abstract

The semiconductor industry continuously aims to increase the transistor density in integrated circuits to improve performance of electronics. As performance and transistor density increases, so does the power density of integrated circuits. To help solve the future demand of thermal management in electronics it is necessary to work with new innovative materials, engineer advanced material structures and develop new cooling concepts. The carbon nanomaterial graphene has the right properties to be used for this purpose as it has an extremely high thermal conductivity and is very lightweight. One challenge with using graphene in thermal management solutions is to engineer macroscopic materials from the nanomaterial graphene without losing too much of the extraordinary properties that are exhibited on nanoscale.

High-performance graphene-based thermal management products are already commercialized today. Products like thermal interface materials (TIMs) and heat spreaders are still novel, and some knowledge gaps exist. More understanding of these products regarding reliability, aging properties and how to optimize production processes can enable them on a broader market. Further, it is believed that graphene-based materials can replace more conventional metals in applications where they have not been used before.

In this thesis, the thermal conductivity and heat dissipation capacity of a graphene-assembled film heat spreader has been shown to be improved by a newly developed annealing process. The effect of the annealing process was demonstrated in a thermal test rig where a high-power light emitting diode (LED) was used as a hot spot while the temperature was monitored with an infrared (IR) camera.

Furthermore, a vertically aligned graphene-based TIM was tested with a new test method to gain a better understanding of the long-term reliability and aging properties. The TIM was subjected to thermal aging, thermal cycling and damp heat while regularly measuring the thermal resistance to see how the performance changes with time. Generally, it could be seen that the thermal resistance was stable, a result that paves way for this type of TIM to be used in applications with a need for high performance over a long time.

Additionally, a literature study on nano-enhanced wick structures was carried out to help determine the most promising nanomaterial-based wick to be used in a two-phase heat spreading device called vapor chamber. Lastly, prototypes of a novel graphene-enhanced vapor chamber were built with graphene assembled film as encapsulating material and they were characterized in a custom-made test rig. The lightweight prototype vapor chambers could outperform a conventional copper vapor chamber in terms of mass-based thermal resistance. However, leak tightness, working fluid and the wick structure were identified as three important future design improvements to further enhance performance and reliability.

Keywords: thermal management, graphene, thermal interface material, reliability testing, heat spreader, vapor chamber, wick structure

List of publications

This thesis is based on the following papers:

I. **Toward ultrahigh thermal conductivity graphene films**
Sihua Guo, Shujin Chen, Amos Nkansah, Abdelhafid Zehri, Murali Murugesan, Yong Zhang, Yan Zhang, Chen Yu, Yifeng Fu, **Markus Enmark**, Jin Chen, Xinfeng Wu, Wei Yu and Johan Liu
2D Materials 10.1 (2023): 014002. **DOI:** 10.1088/2053-1583/ac9421

II. **Reliability Characterization of Graphene Enhanced Thermal Interface Material for Electronics Cooling Applications**
Markus Enmark, Murali Murugesan, Amos Nkansah, Yifeng Fu, Torbjörn, M.J. Nilsson and Johan Liu
2022 IMAPS Nordic Conference on Microelectronics Packaging (NordPac), Gothenburg, Sweden, 2022, pp. 1-6.

III. **A Critical Assessment of Nano Enhanced Vapor Chamber Wick Structures for Electronics Cooling**
Markus Enmark, Yifeng Fu, Torbjörn M.J. Nilsson and Johan Liu
2021 23rd European Microelectronics and Packaging Conference & Exhibition (EMPC), Gothenburg, Sweden, 2021, pp. 1-8. **DOI**: 10.23919/EMPC53418.2021.9584954.

IV. **Design and Characterization of a Novel Graphene-enhanced Vapor Chamber for Lightweight and High-performance Electronics Cooling**
Markus Enmark, Murali Murugesan, Hongfeng Zhang, Torbjörn M.J. Nilsson, Kai J. Kallio, Arian Kamal and Johan Liu
Submitted.

List of acronyms

AFM	-	Atomic Force Microscopy
BLT	-	Bond Line Thickness
CPU	-	Central Processing Unit
DMA	-	Dynamic Mechanical Analysis
GO	-	Graphene Oxide
IR	-	Infrared
LED	-	Light Emitting Diode
SEM	-	Scanning Electron Microscopy
TEM	-	Transmission Electron Microscopy
TGA	-	Thermogravimetric Analysis
TIM	-	Thermal Interface Material
TRL	-	Technology Readiness Level
VC	-	Vapor Chamber
XPS	-	X-ray Photoelectron Spectroscopy
XRD	-	X-ray Diffraction

Table of contents

1. Introduction

1.1 Background

The continuously increasing transistor density in integrated circuits leads to higher power densities and hot-spot temperatures. New innovative materials and more effective thermal management technologies are required to keep up with the cooling demands of advanced electronics. The consequences of insufficient thermal management can be performance loss and shorter lifespan of electronics. Researchers and engineers are constantly working to improve thermal management solutions so that overheating of integrated circuits should not be a bottleneck for performance in any system [1]. Thermal management improvements can be made by different approaches. One alternative is to improve forced convection cooling by raising fan or pump capacity. The downside of this solution is that it also increases the overall power consumption of the thermal management system. A much more sustainable approach would be to lower the overall total thermal resistance between the hot spot and the ambient. In this way, a higher heat dissipation rate can be achieved with less power consumption of the thermal management system. Figure 1 shows an example of a thermal management solution for a central processing unit (CPU) in a desktop. Power consumption of the cooling fan can be minimized with the right technology, optimized design, and appropriate material choices.

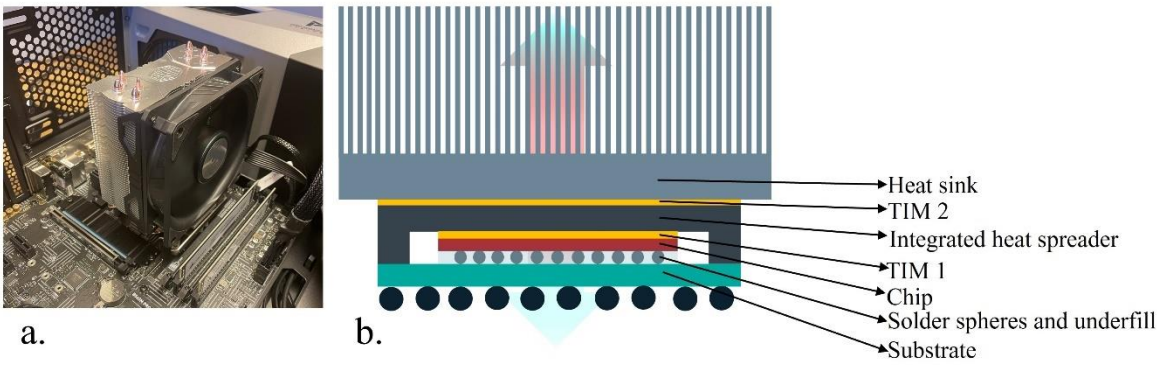

Figure 1: Air-cooling system for a CPU in a desktop with a schematic picture of the different parts in the thermal system. a) Heat sink from Cooler Master Technology inc. with four integrated heat pipes and a fan on top of an Intel CPU in a desktop. b) Schematic of a typical thermal package, showing the main functional parts.

Other design factors that are very important to consider in some applications are size and weight. In hand-held electronics like smartphones and tablets it is important, for the convenience of the user, that the thermal management system does not add unnecessary weight and volume to the device. Furthermore, the weight parameter is also important in electronics which are put in vehicles with a propulsion system. For example, modern automotives, airplanes and satellites have relatively advanced integrated circuits that need cooling. Any extra weight added to such a system will result in unnecessary fuel consumption.

To design thermal management solutions that can reduce the overall thermal resistance of a system and at the same time reduce weight and size, one can make use of new innovative materials. Graphene has proven particularly interesting to use for this purpose. The thermal conductivity of a single layer of graphene can be as high as 5300 W/mK and the density is only 2.01 g/cm^3 when it is assembled into stacked films [2], [3]. Graphene can also be considered a

more sustainable material compared to many metals like copper and aluminum. Sustainable production routes are being researched [4] and since graphene is completely made of carbon it can be easily incinerated and used for energy recovery after end-of-life of the electronic device. It is primarily these properties that make it a perfect alternative to replace metal-based materials and components in thermal management systems. Such materials and components can for example be heat spreaders and TIMs.

Graphene-based heat spreaders and TIMs are recently commercialized products and are gaining market shares from more conventional metal-based thermal management products. Although the performance of many graphene-based products is already good, there are still knowledge gaps that should be filled to improve the products further and enable their use in additional applications.

In this thesis, a new high temperature annealing process was evaluated to create highly thermally conductive graphene-assembled films with a low number of defects and large grain size. Furthermore, one type of graphene-based TIM made from vertically aligned graphene-assembled films in a polymer matrix was tested regarding its reliability and long-term performance when exposed to three standard reliability tests.

A literature study on nano-enhanced wick structures was done to help set the path for future design improvements of wick structures in a two-phase heat spreading device called vapor chamber. The possibility to use graphene-assembled films as encapsulation material in a vapor chamber has also been explored in this thesis. Prototypes of a novel lightweight graphene-enhanced vapor chamber were designed and built by using a graphene-assembled film with high thermal conductivity. The thermal performance of the prototypes was characterized and compared to that of a conventional copper vapor chamber.

1.2 Graphene

Graphene is the central material being evaluated in different thermal management applications in this thesis. It was first discovered by K.S. Novoselov and A.K. Geim who managed to isolate it from graphite in 2004 [5]. Since then it has been target for extensive research to discover its fundamental properties and possible applications [6]. Graphene is one of several different types of carbon nanomaterials. A nanomaterial is according to ISO standard 80004-1:2023, any material with an external dimension between 1-100 nm [7]. Other nanomaterials in the carbon material family are for example fullerenes, quantum dots, carbon nanotubes and nanodiamonds [8].

It is the orbital hybridization state of carbon that determines how the atoms orient to each other to form different carbon structures. Carbon has three different hybridized states *sp*, sp^2 and sp^3. The *sp* hybridization means that the *2s* and one of the *2p* orbitals combine to form the linear *sp* hybridization. Graphene is a 2-dimensional material, meaning that it is only one atom layer thick and is entirely made up of carbon atoms in a hexagonal lattice. The structure of graphene comes from its sp^2 hybridization which means that one *2s* and two *2p* orbitals hybridize to form covalent σ orbitals with neighboring carbon atoms. The remaining *2p* valence orbital orients in the out-of-plane z-direction. This orientation results in a very strong covalently bonded planar hexagonal structure with weaker interlayer Van der waals interactions. The sp^3 hybridization means that all valence orbitals of carbon hybridize to form covalent σ bonds. The tetrahedral orientation of the overlapping orbitals between carbon atoms forms the material known as

diamond. Figure 2 shows a representation of how the carbon atoms orient in a 2-dimensional crystal lattice with sp^2 hybridized covalent bonds to form graphene.

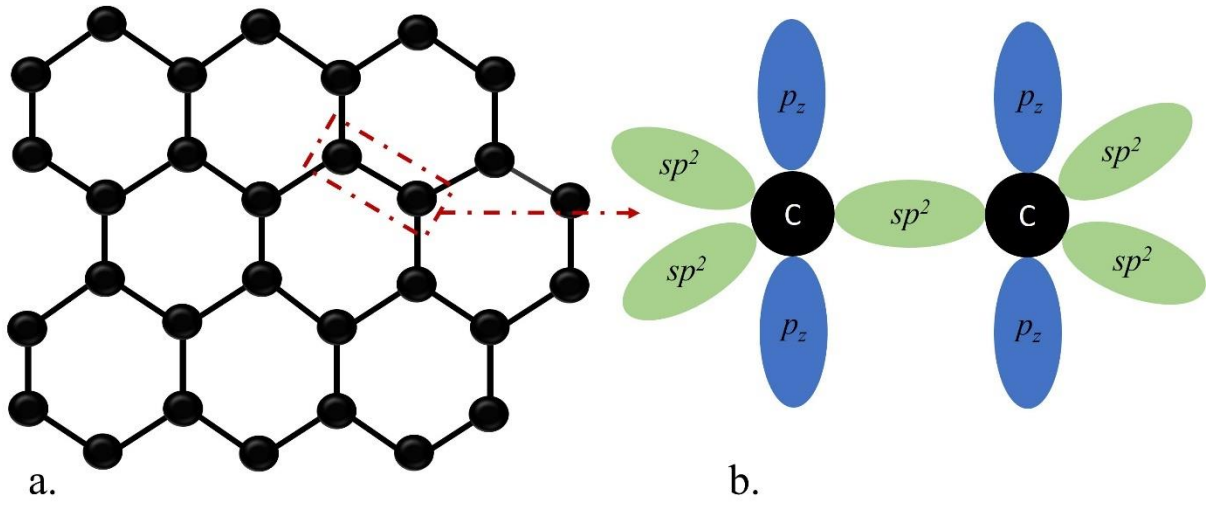

Figure 2: a) Illustration of how the carbon atoms orient in a 2-dimensional hexagonal structure to form graphene. b) Graphene has covalent sp^2 hybridized bonds in-plane while the non-hybridized valence electron forms the out of plane $2p_z$ orbital.

Graphene has been revealed to possess many interesting and valuable properties for different applications. Its mechanical properties such as the extremely high tensile strength and Young's modulus, flexibility and specific surface area make it suitable for many applications such as a composites, flexible electronics and many different bio-medical applications [9]–[12]. It also has very interesting electronic properties. The electrical conductivity is good due to its exceptional carrier mobility, although it is to a certain degree restricted by the relatively low carrier density [13]–[16]. It is however mainly the high thermal conductivity that makes graphene a suitable material to use in electronics thermal management applications. The high thermal conductivity of graphene is due to the strong covalent sp^2 bonds between carbon atoms in the two-dimensional hexagonal lattice that enables efficient heat transport [17]. The heat transport in graphene and other carbon allotropes is, in contrast to metals, governed by lattice vibrations (phonons) instead of electrons [18].

One challenge that researchers and engineers are working with when designing graphene-based thermal management materials is to engineer macroscopic materials from individual graphene flakes without losing too much of the fantastic properties exhibited on nanoscale.

1.3 Graphene in thermal management applications

Graphene can be used in a plethora of different ways in thermal management. Examples are heat spreaders in the form of graphene-assembled films, TIMs of vertically aligned graphene sheets in thermal composites, or as additives in working fluids in two-phase cooling devices such as heat pipes and vapor chambers [2].

1.3.1 Graphene-assembled film heat spreader

The purpose of heat spreaders is to dissipate heat from a device with high power density, like an integrated circuit, to a larger surface area. Traditionally, high thermal conductivity metals like copper or aluminum have been used for this purpose. Currently, companies are trying to move away from using unsustainable metals due to them being a finite natural resource, having

energy intensive production processes and difficulties with recycling after end of life. Lately, graphene-assembled films, also known as graphene paper, have gained popularity to replace metal-based heat spreaders due to their high thermal conductivity, flexibility, low density, and sustainability. Graphene-assembled films are today typically used as thin lightweight heat spreaders in, for example, mobile phones. Although film-like structures made of carbon-based materials have been around for a long time, it is not until recently that the production processes have been adapted so that films with extreme thermal conductivity can be produced.

The well-known Hummers method, which is used to exfoliate graphite into graphitic oxide with a relatively fast and safe procedure, was published in 1959 and already then, film-like structures of graphitic oxide was not a new concept [19]. Further process development has enabled almost complete exfoliation of graphitic oxide to form graphene oxide (GO) dispersions which can be vacuum filtrated into flexible GO films with high fracture strength and high elastic modulus [20]. However, GO film or paper does not possess the thermal conductivity necessary to be used as heat spreaders. Hence, many studies have been conducted to increase the thermal conductivity of GO by for example thermal annealing and mechanical pressing [21]–[23].

N. Wang et al. presented a production method to produce graphene-assembled films with a thermal conductivity as high as 3200 W/mK. This was achieved by precipitation and self-assembly of GO on an aluminum substrate and subsequent dry bubbling to remove the GO film from the substrate. The first step after removal from the aluminum substrate is graphitization at a temperature of 2850°C to remove defects, oxides and increase grain size. In the last step the graphene-assembled film is compressed with a pressure of 300 MPa to reduce interlayer distance and potential air pockets [24]. Efficient and scalable production methods were necessary to fully commercialize graphene-assembled films, this could be achieved by large-scale evaporation of GO-suspension before the annealing and pressing step [25], [26]. The scalable production of graphene-assembled film is illustrated in figure 3.

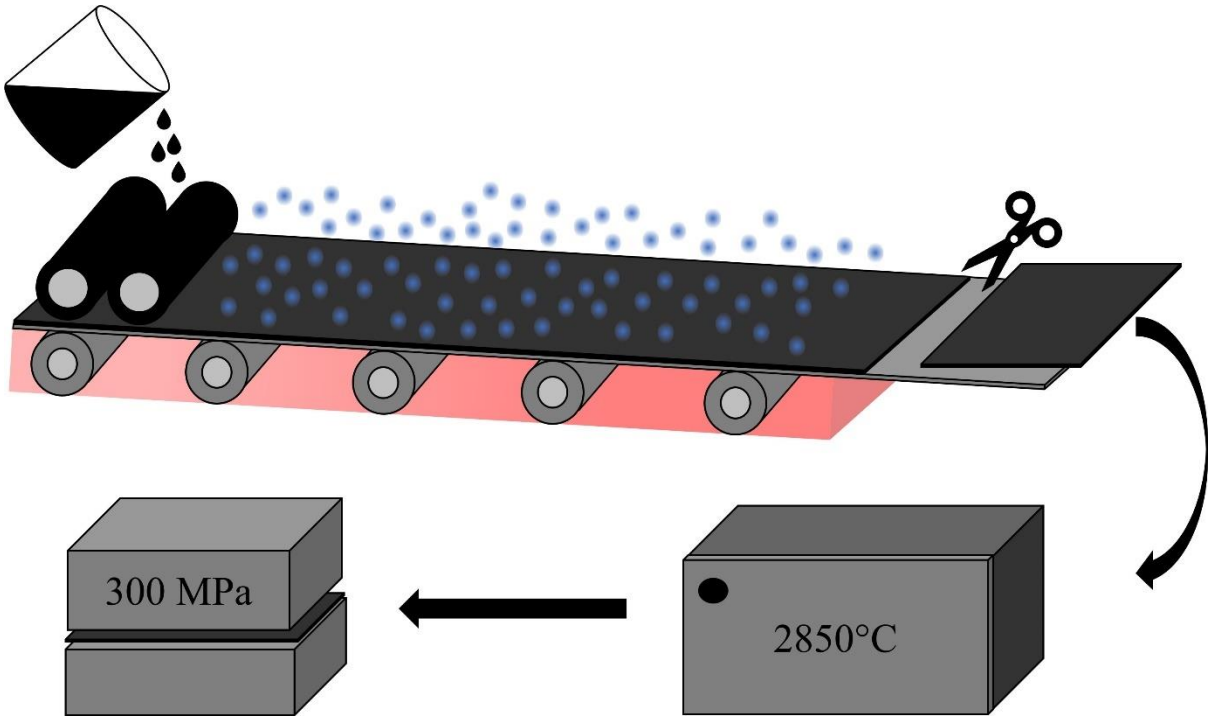

Figure 3: Scalable method for production of GO film by continuous heating and evaporation of solvent. The GO film is further processed by annealing to remove oxides and defects. In the last step the film is pressed to remove any airgaps that might be present and reduce the distance between the graphene layers. Illustration adapted from [26].

SHT Smart High-Tech AB has commercialized this method and can provide highly thermally conductive graphene-assembled films for heat spreading in electronics [27]. These graphene-assembled films have been used and evaluated in this thesis. Figure 4 shows scanning electron microscope (SEM) pictures of a graphene-assembled film heat spreader after annealing and mechanical pressing. The 100 µm thick sample is viewed from above and in cross-section.

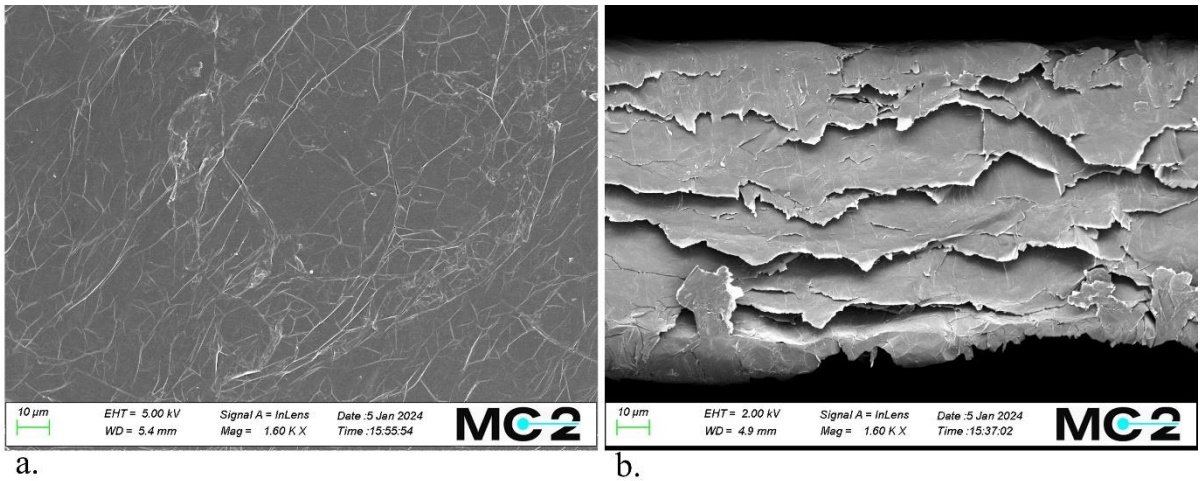

a. b.

Figure 4: a) Top view of graphene-assembled film after annealing and mechanical pressing. b) Cross-sectional view of a 100 µm thick graphene-assembled film after annealing and mechanical pressing.

1.3.2 Graphene-based thermal interface materials

The purpose of a TIM is to facilitate heat flux between two solid surfaces. In electronics, this is often necessary between the integrated circuit and the integrated heat spreader or between the integrated heat spreader and the heat sink as is shown in figure 1. The performance of a TIM can be expressed by the total thermal resistance R_{tot} between two solid surfaces. Characterization of R_{tot} can be done by measuring the temperature difference, ΔT, over the interface and divide it by the total power input Q.

$$R_{tot} = \frac{\Delta T}{Q} \tag{1}$$

Furthermore, it is known that R_{tot} depends on contact resistances, R_{c1} and R_{c2}, as well as the bond line thickness (BLT) and the intrinsic thermal conductivity, λ, of the designed TIM.

$$R_{tot} = R_{c1} + R_{c2} + \frac{BLT}{\lambda} \tag{2}$$

Hence it is important that the TIM is thin, has high cross-plane thermal conductivity, and low thermal contact resistance to have as low total thermal resistance as possible. Figure 5 shows how a TIM facilitates heat transport by filling the air gaps between two surfaces with a highly thermally conductive material.

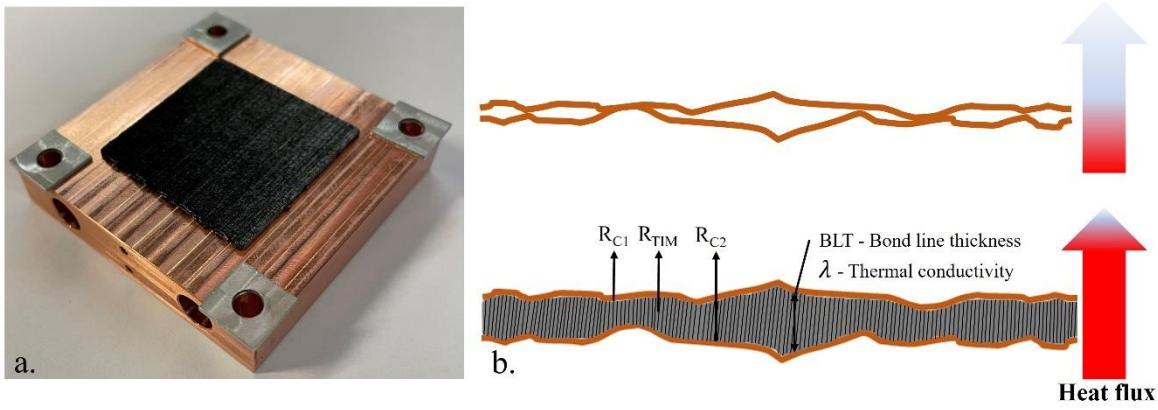

Figure 5: a) A thermal pad made from vertically aligned graphene in a polymer matrix on a copper substrate used for testing thermal resistance of the TIM. b) Schematic picture of how a TIM facilitates heat flux by filling air gaps between two solid surfaces.

There are many different categories of TIMs including for example, thermal grease, thermal pads, phase change materials, gels, thermal conductive adhesives, liquid metals and solders [28]. A thermal pad, like the one shown in figure 5, is a type of composite based on a polymer matrix and a thermally conductive filler material. Different carbon allotropes like graphene and carbon nanotubes have shown great potential to be used as filler material in thermal composites to replace ceramic or metallic conductive fillers. Carbon nanotubes first attracted the most attention and were extensively studied to be used in different polymer matrices [29], [30].

However, comparison studies between graphene and carbon nanotubes have shown that graphene can give a higher thermal conductivity at the same filler fraction and is both easier and cheaper to produce compared to carbon nanotube-based composites [28], [31]. The thermal pad seen in figure 5 is made of vertically aligned graphene in a polymer matrix. As is illustrated in figure 5(b), the thermal conductivity between two solid surfaces is maximized in the cross-plane direction by aligning the graphene sheets vertically.

Some important factors to consider when designing graphene-based thermal composites include fill level of graphene, quality of the graphene flakes as well as alignment of graphene flakes in the polymer matrix [28], [32]. There are also many different techniques to produce graphene-based thermal composites. One method which has proven to be successful is to make use of vertically aligned graphene-assembled films in a laminated structure together with a polymer binder. With this technique, it has been shown that a flexible thermal pad with a graphene volume ratio of 75% could reach thermal conductivities of 1379 ± 138 W/mK. However, it was also seen that a pad with lower filler content gave better contact resistance and thereby lower total thermal resistance [33]. The optimum relation between thermal conductivity and contact resistances became an engineering problem to tailor the graphene filler content and the ductility of the polymer to find the properties that gives the lowest total thermal resistance.

1.3.3 Graphene and other nanomaterials in vapor chambers and heat pipes

Vapor chambers and heat pipes are other types of heat spreaders than the ones described in section 1.3.1. Instead of transporting heat via a solid material like the graphene-assembled film, they utilize the latent heat of vaporization and condensation of working fluids to effectively dissipate heat from a hot spot. Vapor chambers work in the two-dimensional plane and are put on top of a hot spot to spread heat over a larger area. Heat pipes instead work in one dimension and transports heat from a hot spot to another location like a heat sink. The working principles of vapor chambers and heat pipes are the same. They are put adjacent to a heat generating device and when heat is supplied it evaporates an encapsulated working fluid in the cavity of the vapor chamber or heat pipe. The evaporated fluid then spreads to the colder parts of the device and as it cools down it condenses and flows back to the hot part of the device via capillary forces in a wick inside the cavity [34]. The working principles of a vapor chamber and the three most common wick structures are illustrated in figure 6.

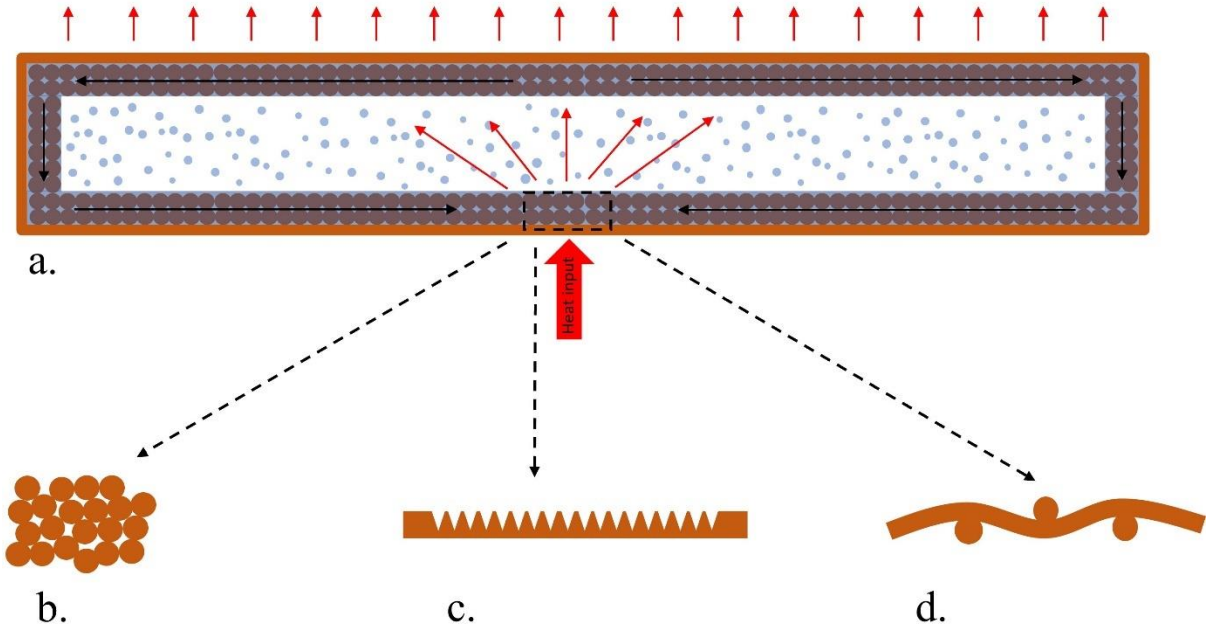

Figure 6: Graphical illustration of a vapor chamber with three different types of wicks. a) Schematical picture of a vapor chamber in cross-section. Working fluid is evaporated where the heat is supplied and the vapor spreads to the colder side of the vapor chamber where it condenses. The condensed fluid is transported back to the hot spot via capillary forces. b) Sintered wick. c) Grooved wick. d) Meshed wick.

Graphene is only one of many nanomaterials that have been studied to be used to enhance the performance of vapor chambers and heat pipes. The most common application is to make use of nanofluids as working fluid to increase its thermal conductivity [35]–[39]. This has been a successful approach to increase the performance of vapor chambers, at least momentarily. However, one problem with nanofluids in vapor chambers and heat pipes can be that particle suspensions tend to agglomerate and deposit to the vapor chamber wall and wick. Agglomeration leads to performance degradation over time [40]. Another approach is to target the wick of the vapor chamber or heat pipe to improve capillary performance, wettability, and the thin film evaporation process. This can be achieved by many different techniques, ranging from nano structuring of metal wicks by different chemical processes, carbon aerogels, carbon nanotube patterns and nanoparticle coatings.

One limitation of graphene in vapor chamber working fluids, wicks, and envelope applications is its water wettability properties. Figure 7 shows a contact angle comparison between water and ethanol on graphene-assembled film. The large contact angle of the water droplet shows that graphene is hydrophobic. The hydrophobic properties of graphene can hinder its use in vapor chambers and heat pipes. A good wettability is required for obtaining a good nanoparticle suspension as well as good heat transfer characteristics between wick or envelope and the working fluid. It is important that the hydrophobicity problem is addressed since water is a very common and effective working fluid in vapor chambers and heat pipes which are intended to work in environments above 0 °C. GO is much easier to use and does not require complicated fabrication procedures or surfactants when the nanofluid suspension is prepared. When evaluated as a coating on a sintered copper wick in a heat pipe, GO has been seen to increase thermal performance of the device [41]. Despite the poor wettability properties of graphene, a graphene-distilled water suspension has also been studied to be used as working fluid. Mehrali

et al. showed how high power ultrasonication could facilitate preparation of a stable graphene suspension. The ultrasonication process created homogeneous graphene dispersions that were seen to be stable for at least 600 h. Furthermore it could be seen that such graphene dispersions could increase the fluids thermal conductivity by 28 % compared to distilled water [42]. When applied in a heat pipe with a sintered copper wick the graphene dispersion was shown to decrease the thermal resistance of the heat pipe with up to 48 % [43]. Furthermore, one study has been carried out to evaluate the possibility of using graphene-assembled film as envelope material in a heat pipe. In this study, ethanol was used as working fluid instead of water. It was shown that the graphene-based heat pipe could outperform similar copper devices in terms of heat dissipation capacity per unit mass due to the high thermal conductivity and low density of the graphene-assembled film [44].

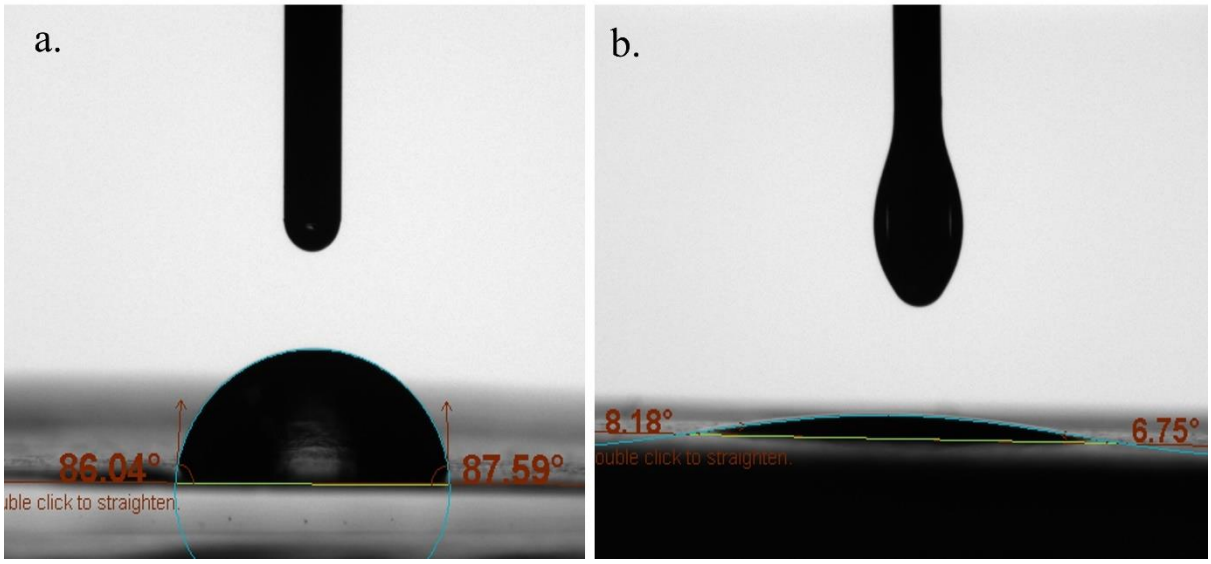

Figure 7: Wettability of two different working fluids on graphene-assembled film. a) Contact angle of water on graphene-assembled film. b) Contact angle of ethanol on graphene-assembled film.

1.4 Scope of this thesis

Graphene-based products are being introduced on the commercial market on a broader scale. One particularly interesting application is thermal management in electronics due to the suitable material properties of graphene. Some graphene-based thermal management applications have already been introduced on the market. However, the applications are still novel, and more research and development can further enhance knowledge and performance of these products. Graphene is still a rather new material and exploring new applications of graphene in thermal management can also further widen the range of applications where the beneficial properties of graphene can be exploited.

1.4.1 Graphene-assembled film heat spreaders

Developing and optimizing fabrication processes of graphene-assembled film heat spreaders can improve its thermal conductivity. Higher thermal conductivity paves way for better heat spreading properties in thermal management applications and can possibly also open for usage in new applications. In this thesis graphene-assembled film is fabricated with a new high temperature annealing

process and the thermal conductivity, structural properties and heat dissipation performance are characterized after production.

1.4.2 Vertically aligned graphene thermal interface materials

There are many types of graphene-based TIMs. One of them is the vertically aligned graphene TIM described in section 1.3.2. It is gaining popularity due to its high thermal conductivity, which can help to achieve a low total thermal resistance in a thermal package. Another advantage with this type of thermal composite is that it should not dry out as quickly compared to thermal grease and therefore it can maintain a high thermal performance over a longer time. However, reliability and aging aspects of graphene-based TIMs are not well researched and standardized methods for evaluating these aspects are lacking. In this thesis a new method to characterize thermal resistance degradation of thermal pads over time is presented. The method is used to characterize a vertically aligned graphene thermal pad. This is done in three different standard aging tests, thermal aging, damp heat, and thermal cycling.

1.4.3 Nano-enhanced vapor chambers

Possible new applications for graphene and graphene-assembled films are heat pipes and vapor chambers. In this thesis, a literature study is done to explore the most promising materials and structures to implement as a wick in a vapor chamber to improve liquid and thermal transport properties and ultimately overall performance of the vapor chamber. Furthermore, graphene-assembled film is evaluated to be used as encapsulating material in vapor chambers. A set of novel graphene-enhanced vapor chambers were designed and fabricated. The graphene-enhanced vapor chambers are also benchmarked against a commercial copper vapor chamber in a new customized test rig for thermal resistance characterization of vapor chambers.

2. Fabrication of graphene-assembled films with ultra-high thermal conductivity

Recently developed fabrication methods have improved the thermal conductivity of graphene-assembled films and thereby enabled them to be used as heat spreaders in electronics instead of more conventional copper films. Successful fabrication procedures involve high temperature annealing of graphene-oxide with a subsequent pressing step [24]. The process parameters of graphene assembled film fabrication can be further optimized to achieve the highest possible thermal conductivity. This chapter is based on paper I in which it is shown that a 1 μm thick graphene-assembled film with a thermal conductivity of 3826 W/mK can be produced with a two-step temperature annealing process and subsequent mechanical pressing.

2.1 Method

Production of the graphene-assembled film started with expanded graphite as precursor. The expanded graphite was treated with the modified Hummer's method to obtain a graphene-oxide solution. The GO suspension was then mixed with a high shear mixer and centrifuged to obtain a homogenous and fine dispersion of GO sheets. The solid film was prepared by precipitation and self-assembly of the GO sheets into a film like structure while simultaneously evaporating the solvent.

The subsequent thermal annealing was carried out in two steps. The film was first subjected to a temperature of 1500 °C to create a reduced GO film by eliminating oxides. The second step in the thermal annealing process was carried out at a temperature of 2850 °C and aimed to create a highly crystalline graphene hexagonal lattice without atomic vacancies from the previously removed oxides. In this production step, different annealing times were used to be able to evaluate the effect of annealing time on thermal conductivity, number of defects and grain size. The annealing times tested for the reduced graphene films were 1, 2, 3 and 4 hours. Last of all, the annealed films were compressed with a pressure of 300 MPa to mechanically remove interlayer voids.

Several characterization methods were used to assess the quality of the produced graphene-assembled films. First, defect rate and residual oxide groups were analyzed with x-ray diffraction (XRD), x-ray photoelectron spectroscopy (XPS), and Raman spectroscopy. Then the structural properties were evaluated by SEM, transmission electron microscopy (TEM) and atomic force microscope (AFM). Lastly the thermal conductivity was measured with the Joule self-heating method [22], [45]–[47].

2.2 Results and discussion

The thermal conductivity measurements of the graphene-assembled films showed that longer annealing time at 2850 °C gives higher thermal conductivity. The results from the Joule self-heating measurements can be seen in figure 8.

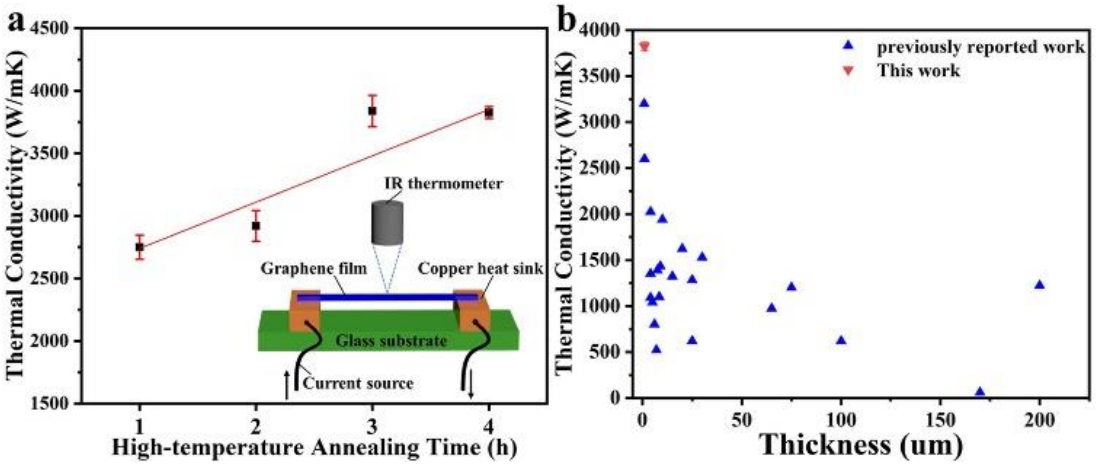

Figure 8: a) Thermal conductivity as function of annealing time of 1 µm thick graphene-assembled films. b) Thermal conductivity measured in this work compared to previously reported values for graphene-assembled films. Figures and data from paper I. Licensed under CC BY 4.0.

The fact that thermal conductivity increases with annealing time can be explained by an increase in crystallinity and a decrease in number of defects with longer annealing time. A more perfect crystal lattice facilitates unimpeded phonon transport. The degree of crystallinity and number defects could be confirmed in the structural analysis by the different spectroscopy and microscopy methods outlined in 2.1.

A graphene-assembled film with 25 µm thickness, produced in a similar way as the samples in figure 8, was used in a benchmark test and compared with a non-annealed GO film with same thickness to demonstrate the practical effects of the annealing process. The test setup and results are shown in figure 9.

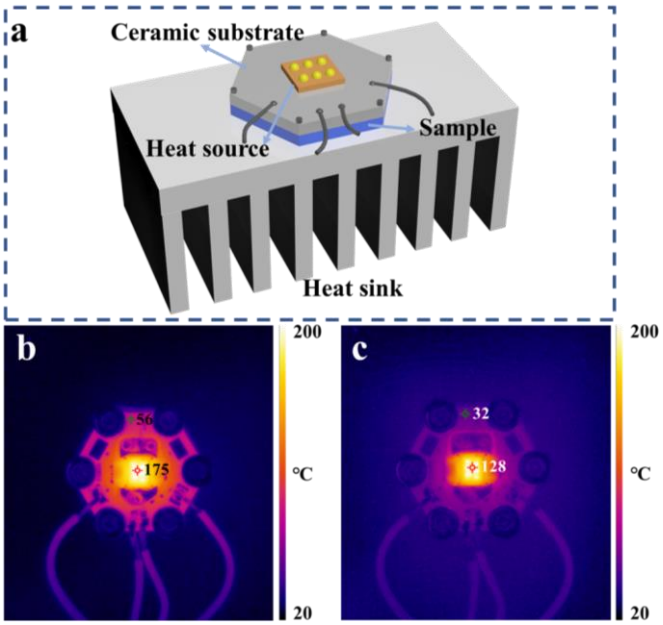

Figure 9: a) Thermal test platform for demonstrating performance of TIMs and heat spreaders. b) Temperature distribution when using a non-annealed GO film. c) Temperature distribution for high temperature annealed graphene-assembled film. Figures and data from paper I. Licensed under CC BY 4.0.

Figure 9(a) shows the test setup used for comparing the non-annealed GO film to a graphene-assembled film which had been annealed at 2850 °C. The thermal test platform consists of an LED on a ceramic substrate which is assembled on a heat sink with screws using constant torque. The heat spreading material was put underneath the substrate carrying the LED. The temperature of the LED and the substrate was monitored with a thermal IR camera of model FLIR A655. By comparing figure 9(b) to 9(c) - it can be seen that the heat transfer to the heat sink is more effective for the graphene-assembled film. This results in a significantly lower hotspot temperature without changing the fan speed. A result that clearly demonstrates the energy saving possibilities that can be achieved by engineering materials with high thermal conductivity. The lifetime of LEDs and electronics in general will be extended when they are operating at lower temperatures.

2.3 Conclusions and outlook

Longer annealing time at high temperature has a positive effect on thermal conductivity of graphene-assembled films. The improvement in thermal conductivity is because a longer annealing time enables elimination of more oxides and defects and thereby creating a very crystalline hexagonal sp^2 hybridized carbon structure for unimpeded phonon transport.

This finding is important because it gives a better understanding of how to tune production parameters for optimizing thermal conductivity. The fact that the thermal conductivity of graphene-assembled films can be enhanced by using longer annealing times can possibly also speed up a shift away from using copper as heat spreaders and instead use graphene-assembled film if the process is still economically competitive. Furthermore, there is a possibility that new applications can be found for graphene-assembled films with ultra-high thermal conductivity. One example of a new application area is vapor chambers.

A similar thermal conductivity was achieved for 3- and 4-hours annealing times in this work. Given the variance of the thermal conductivity it is not certain that 3 or even 4 hours will result in the maximum possible thermal conductivity. Future studies on graphene-assembled films could possibly explore the physical limits of thermal conductivity by either extending processing time or increasing the temperature even more. In the end, production of graphene-assembled films will become a cost-performance issue to decide if the increase in thermal conductivity is worth the energy cost of the extra annealing time.

3. Reliability study of a graphene-based thermal interface material

Vertically aligned graphene-based thermal pads are already commercially available. One example is the pad seen in figure 5 which is developed and sold by SHT Smart High-Tech AB [27]. Research and development have previously been focused on thermal characterization, improvement of thermal conductivity and lowering thermal contact resistance. It is believed that one of the advantages of this type of TIM, apart from its high thermal conductivity, is its constant performance over time. In theory, graphene-polymer composites should not be as susceptible to dry out compared to for example thermal paste. This is a desirable characteristic in many applications where you want to avoid changing TIM on a regular basis to prevent overheating of integrated circuits.

How the performance of graphene-based thermal pads changes over time has up until now not been thoroughly investigated. Guo et al. states that, even though the performance of new carbon-based TIMs have been proven to be good, future research and development needs to focus on endurance and reliability [48]. One challenge with reliability testing of TIMs is the accelerated aging process. TIM manufacturers today often rely on TIM characterization methods like ASTM D5470-17 to measure thermal resistance or ASTM E1461 to measure thermal conductivity. Potential reliability problems are therefore not found until after the product has been used for some time in the actual electronics application. Generic test methods to test the thermal resistance in accelerated aging tests are lacking. It is desirable to be able to monitor the thermal resistance of the TIM during the accelerated aging test. Having to remove the TIM from its compressed state, measure the thermal resistance and put it back to continue the aging test introduces extra uncertainties. To solve this problem, a test method was developed to be able to measure the thermal resistance of a TIM without having to remove it from the thermal test rig. This method was applied to a vertically aligned graphene-based thermal pad and three different standard environmental aging tests were run, damp heat, thermal cycling, and thermal aging. This chapter is based on the work in paper II.

3.1 Method

The vertically aligned graphene-based thermal pads were assembled in customized copper thermal test rigs with a 30% compression. This could be achieved by aluminum spacers that were placed in each corner of the thermal test rigs. The aluminum spacers had a thickness that was tailored to give a 30% compression of all thermal pads regardless of initial thickness. Test rigs before and after assembly are shown in figure 10.

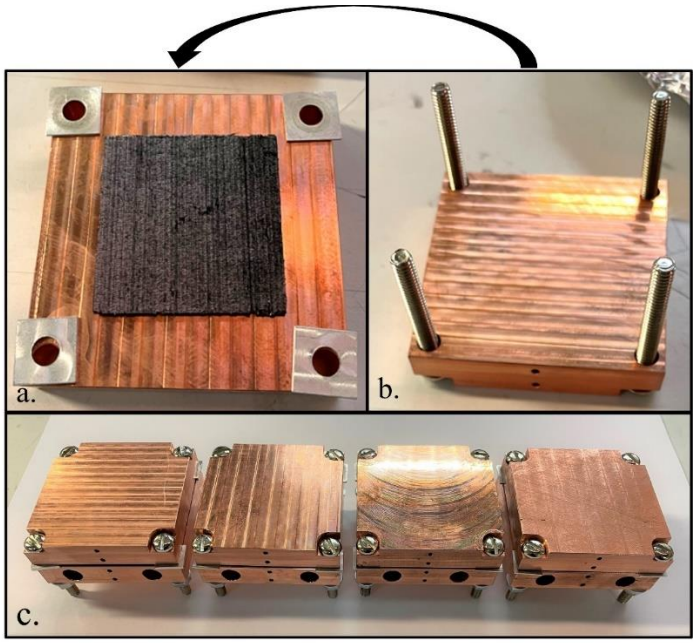

Figure 10: Thermal test rigs before and after assembly. a) Vertically aligned graphene-based thermal pad on a heater block with aluminum spacers in each corner. b) Upper part, used to apply compression to the thermal pad with stainless steel screws in each corner. c) Assembled thermal test rigs before starting an accelerated aging test.

Three different accelerated aging procedures were run, damp heat, thermal cycling, and thermal aging. Four thermal test rigs were run in each reliability test, they contained three thermal pads with original thicknesses of 0.8, 1.0, and 2.0 mm as well as one empty rig. The empty rig was included to see if a measured change in thermal resistance was due to the TIM or the test rig itself. It also made it possible to exclude the contribution of the test rig in terms of thermal resistance (screws and spacers) to only get the thermal resistance of the TIM.

All test specimens were characterized before starting the accelerated aging procedures. This was done by applying heat with two 50 W heaters in the bottom part of the thermal test rig and measuring the temperature difference over the TIM. The entire test setup was encapsulated in Styrofoam during the measurement to minimize convection losses to the ambient. The test setup was cooled by clamping a water-cooled heat sink on top of the thermal test rig with a constant torque. The water-cooled heat sink was driven by an Alphacool VPP655 water pump providing a constant flowrate. A schematic of the test setup is illustrated in figure 11.

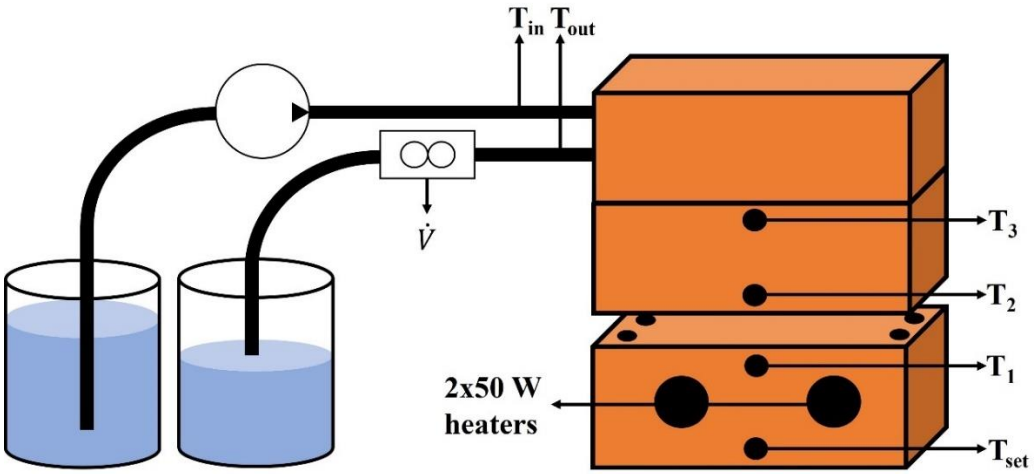

Figure 11: Schematic of test setup for characterizing thermal resistance of the TIM when compressed in the thermal test rigs.

After characterizing the TIMs, the thermal resistance was calculated according to equation 1 where ΔT in this case was the temperature difference between T_1 and T_2 and Q was the power input of 100 W. After thermal resistance characterization the thermal test rigs were put in the respective reliability test. They were then taken out of the oven or conditioning chamber at regular intervals to redo the characterization. In this way the change in performance of the TIM could be seen by plotting the thermal resistance against aging time. The intermittent characterization and accelerated aging is depicted in figure 12.

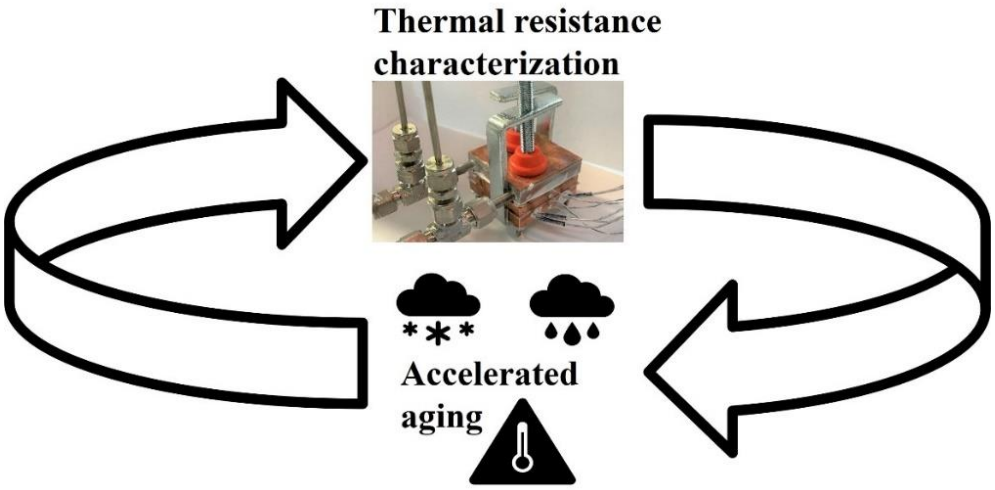

Figure 12: The thermal test rigs were removed from the respective accelerated aging test at regular intervals to do the thermal characterization.

The measured thermal resistance accounts for both the thermal test rig itself and the TIM due to the contact points in each corner which provide a path for thermal conduction. However, the thermal resistance contribution from the rig can be subtracted from the measured total thermal resistance by the following equations of parallel thermal resistances:

$$\frac{1}{R_{tot}^{Ref}} = \frac{1}{R_{spacers}} + \frac{1}{R_{air}^{Ref}} \tag{3}$$

$$\frac{1}{R_{tot}^{TIM}} = \frac{1}{R_{spacers}} + \frac{1}{R_{air}^{TIM}} + \frac{1}{R_{TIM}} \tag{4}$$

$$R_{TIM} = \frac{1}{\frac{1}{R_{tot}^{TIM}} - \frac{1}{R_{spacers}} - \frac{1}{R_{air}^{TIM}}} \tag{5}$$

This calculation could be done for the 1 mm thick TIM since this rig had the same spacer thickness as the reference rig. It should be noted that this calculation is an approximation that neglects the contribution of convection and radiation on the different thermal resistances.

3.2 Results and discussion

The measured thermal resistance could be plotted against time or number of thermal cycles in the respective reliability test. The results of how the thermal resistance changes over time are shown in figure 13.

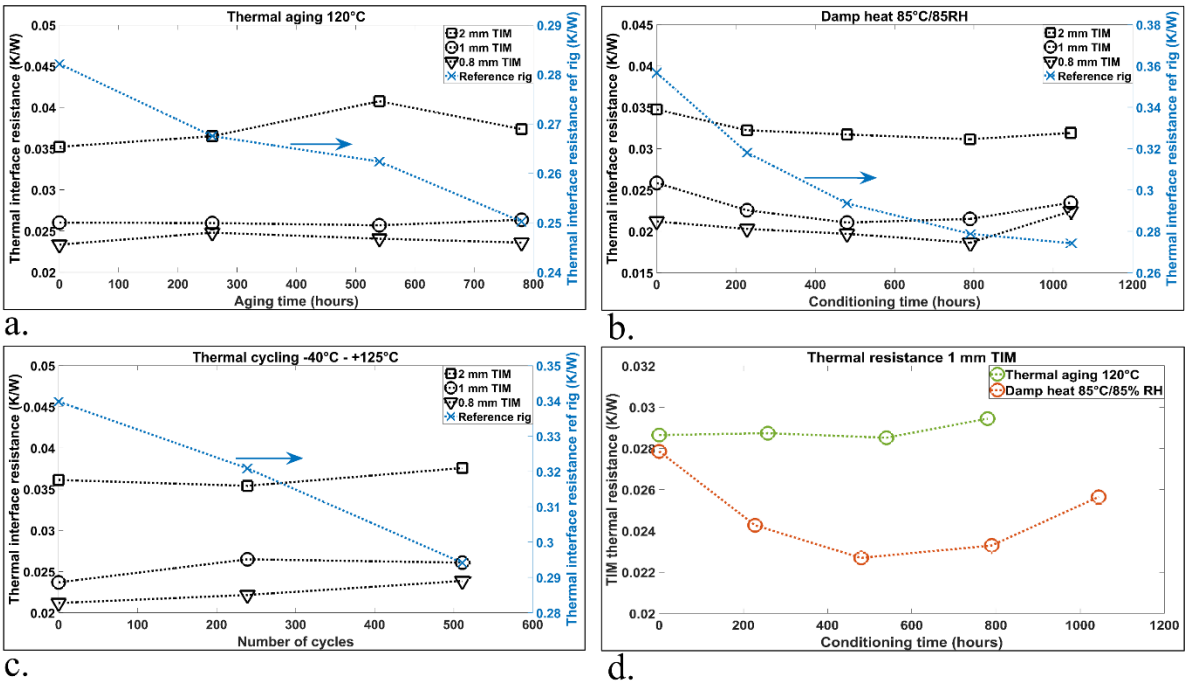

Figure 13: Thermal resistance as function of test time or number of cycles for the different reliability tests. a) Results from the thermal aging test. b) Results from the damp heat test. c) Results from the thermal cycling test. d) Thermal resistance as function of conditioning time in the thermal aging and damp heat test after removing the contribution of the test rig. The results are for the 1 mm thick pad.

Figure 13 reveals many interesting results that can be discussed in more detail. First, the thermal resistances in all reliability tests are rather stable over time even though the thermal

resistances of the empty reference rigs are decreasing. The decreasing thermal resistance of the reference rigs is most likely due to that the thermal contact resistance between the aluminum spacer and the copper blocks decreases with time in all three environments. Hence it was important to be able to exclude the thermal resistance contribution of the test rigs. In hindsight it would have been better to instead make use of ceramic spacers to avoid improved intermetallic contact resistance over time. Figure 13(d) shows the thermal resistance of the thermal pads after removing the contribution of the test rigs. In the thermal aging test, the performance of the TIMs is very stable over time. In the damp heat test however, the thermal resistance initially decreases and after somewhere between 480- 790 hours it starts to increase. There can be several potential explanations for this. The fact that the same trend cannot be seen in thermal aging tells us that the phenomena have to do with moisture. The pad is a graphene-polymer composite with a high graphene content. One potential explanation for the initial decrease in thermal resistance is swelling. At this point it is not known how much moisture the polymer can absorb and if the graphene sheets can provide a pathway for increased water diffusion and swelling of the thermal pads. If the pad swells, which is anticipated for a polymer composite, then the thermal contact resistance should decrease due to an increase in pressure on the pad from the test rig. Other possible explanations for the initial decrease of thermal resistance are if the damp heat environment can facilitate further post curing of the polymer or if water can fill airgaps between the pad and the copper surface and thus decrease thermal contact resistance. At this point it is also unknown how potential water uptake in the thermal pad would affect its thermal conductivity. It could theoretically contribute to an increase in thermal conductivity since the thermal conductivity of water is higher than that of the polymer. At some point between 480 and 790 hours the degrading mechanisms become greater than the initial positive effects of moisture and thus the thermal resistance starts to increase again. The degrading effects can potentially be due to that moisture and heat degrades the polymer and compression set that ultimately lowers the force acting on the pad.

By comparing the thermal resistances of the 1 mm thick TIM from figure 13(a-c) to the thermal resistance in figure 13(d), one can see that the difference is quite small. This means that the contribution to heat transfer from the screws and spacers is small. The contribution could have been even lower if ceramic spacers and screws with a lower thermal conductivity were used instead of metal. A change to ceramic spacers could potentially also have made the thermal resistance of the reference rigs more constant over time.

The change in thermal resistance at the end of each reliability test is summarized in table 1.

Table 1: Change in thermal resistance at the end of each reliability test compared to the pristine thermal pads.

	Thermal aging 780 h	**Damp heat 1044 h**	**Thermal cycling 511 cycles**
Ref rig	-11 %	-23 %	-13 %
0.8 mm TIM	+1 %	+6 %	+13 %
1 mm TIM	+1 %	-9 %	+10 %
2 mm TIM	+6 %	-8 %	+4 %

Table 1 shows that the change in thermal resistance is generally small meaning that this vertically aligned graphene thermal pad has a good reliability in terms of thermal performance over time. Change in thermal resistance was generally the lowest for the thermal aging samples

and highest for the thermal cycling samples. The thermal resistance of the 1 and 2 mm thick samples that were subjected to damp heat even showed an improvement in thermal resistance.

3.3 Conclusions and outlook

Thermal resistance of a vertically aligned graphene thermal pad was shown to be very stable when subjected to standard reliability tests like thermal aging, damp heat and thermal cycling. The thermal cycling test affected the thermal pads the most while very little effect could be seen in the thermal aging test. Moisture was seen to have an initial positive effect on thermal resistance of the tested pads. The developed test method was deemed promising for future reliability studies of thermal pads. The fact that the compression rate could be kept constant led to the possibility to study how effects such as swelling, and compression set could affect the performance. It was also seen that the contribution from the screws and spacers was relatively small. However, it is worth noting that it can be made even smaller by using ceramic screws and spacers.

The very stable performance of the vertically aligned graphene thermal pads opens for replacing other less stable TIMs such as thermal paste in applications where long-term high performance is important. This could for example be applications where it is complicated and time-consuming to replace a TIM.

In this study it was shown that the thermal resistance is very stable over time. However, that does not say anything about how the mechanical properties and chemical composition of the pads change over time. To supplement this study, it would be of interest to do more analysis on the thermal pads after finishing the reliability tests and removing them from the thermal test rigs. Such tests could include compression set measurements, thermogravimetric analysis (TGA) and dynamic mechanical analysis (DMA). Information about change in chemical composition, elastic modulus and compression set could give a better understanding about the underlying mechanisms of performance change.

4. Nano-enhanced vapor chambers

The performance of vapor chambers can be improved by implementation of nanotechnology. Many studies have shown that nanoparticles can significantly improve thermal conductivity of the working fluid [35]–[39]. It has also been shown that nanostructures on vapor chamber and heat pipe wicks can reduce the thermal resistance in the evaporator region by improving thermal conductivity, capillary performance, thin-film area for evaporation and increasing the number of nucleation sites on the wick [49]–[51]. This chapter is based on paper III and IV. First, based on the work in paper III, a literature study on nano-enhanced vapor chamber wick structures is presented. This literature study can act as a guide to set the plan for future work on how to improve the performance of the graphene-enhanced vapor chambers by nanostructured wicks. Then, based on the work presented in paper IV, a new lightweight vapor chamber concept is introduced. Prototypes of novel graphene-enhanced vapor chambers have been designed and built by using graphene-assembled film as envelopes. The graphene-enhanced vapor chambers have been compared to an existing copper vapor chamber in terms of thermal resistance in a customized test setup for vapor chamber characterization.

4.1 Literature study on nano-enhanced wick structures

One of the most important parts of a vapor chamber is the wick structure since it controls the evaporation process and transports working fluid to the evaporator. An efficient wick should provide enough liquid to the evaporator to prevent dry-out while maintaining an efficient boiling process. To design an optimum wick structure is challenging. There are many parameters that need to be accounted for and some of them are even conflicting, which means that trade-offs are needed. To get a better understanding of how to design a good wick structure this chapter will start with some underlying theory.

4.1.1 Design guidelines of wick structures

Vapor chambers and heat pipes have an operating condition that needs to be fulfilled to prevent liquid dry-out in the evaporator. The operating condition is given in equation 6 [52].

$$\Delta P_c \geq \Delta P_{liq} + \Delta P_{vap} + \Delta P_g \tag{6}$$

The operating condition says that the capillary pressure ΔP_c must always be greater than or equal to the sum of the liquid pressure drop ΔP_{liq}, vapor pressure drop ΔP_{vap} and the gravity assisted pressure drop ΔP_g. The reader is referred to paper III for an in-detail explanation of the parameters in equation 6.

Faghri [52] states that three parameters are governing for the performance of a wick in a vapor chamber or heat pipe. These parameters are capillary radius, permeability, and effective thermal conductivity of the wick. A small capillary radius will provide a high capillary pressure; however, it will also impact the permeability of the wick and increase the liquid pressure drop. Therefore, there is a limit on how small the capillary radius can be in a wick before the evaporator starts to experience liquid dry-out due to insufficient permeability. Hence, wick designers have tried to solve this trade-off by working with hybrid wicks. A hybrid wick has different properties in the adiabatic section and the evaporator. The condenser and adiabatic section benefits from a larger capillary radius to achieve a higher permeability while the evaporator can have a smaller capillary radius [53]. However, care must be taken not to introduce vapor pockets in the evaporator. Vapor pockets are a phenomenon that can occur if a

homogenous wick with too small pore size is used, and it will result in obstructed liquid transport. To solve this problem, it has been shown beneficial to make use of wicks with different pore sizes, so called bi-porous wicks. The bigger pores allows for degassing while the smaller pores gives the desired capillary pressure [54].

4.1.2 Nano-enhanced wick structures

Nanomaterials can contribute with several different advantages in wick structures compared to conventional materials. Thermal conductivity, low density, nanoscale pore size, superhydrophilicity and superior thin film evaporation processes are some of the advantages that can be achieved.

In paper III the reviewed studies were divided into five different wick categories depending on the studied nanomaterial. The different categories were carbon nanotube wicks, graphene coated wicks, nanoparticle coated wicks, nanostructured metal wicks and nanomaterial aerogel wicks. Three different types of nano wicks are illustrated in figure 14.

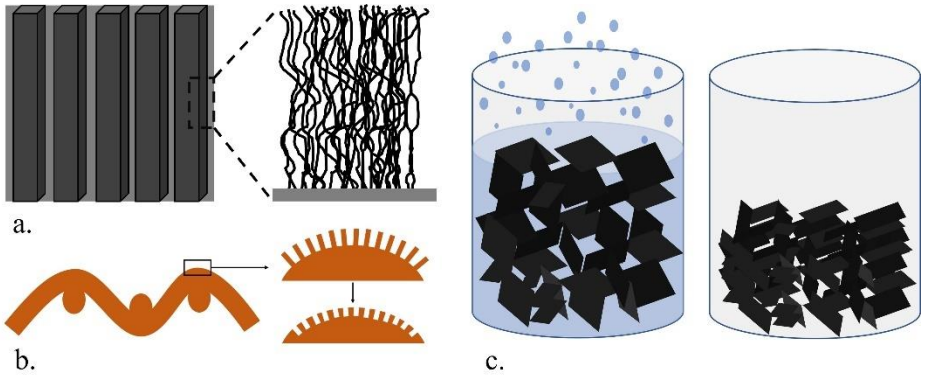

Figure 14: Illustration of 3 different types of nano wicks. a) Patterned carbon nanotube forests on a silicon substrate as grown by Cai et al. [55]. *b) Chemically etched copper mesh to create nanograss on copper mesh as fabricated by Wen et al.* [56]. *c) Graphene aerogel fabricated by evaporation of the water solvent and subsequent supercritical drying as done by Jung et al.* [57].

One of the objectives of this literature study was to find the most promising nano wick to incorporate in novel vapor chambers. To achieve that, the papers covered in the literature study were plotted against their respective publication year. The results are shown in figure 15.

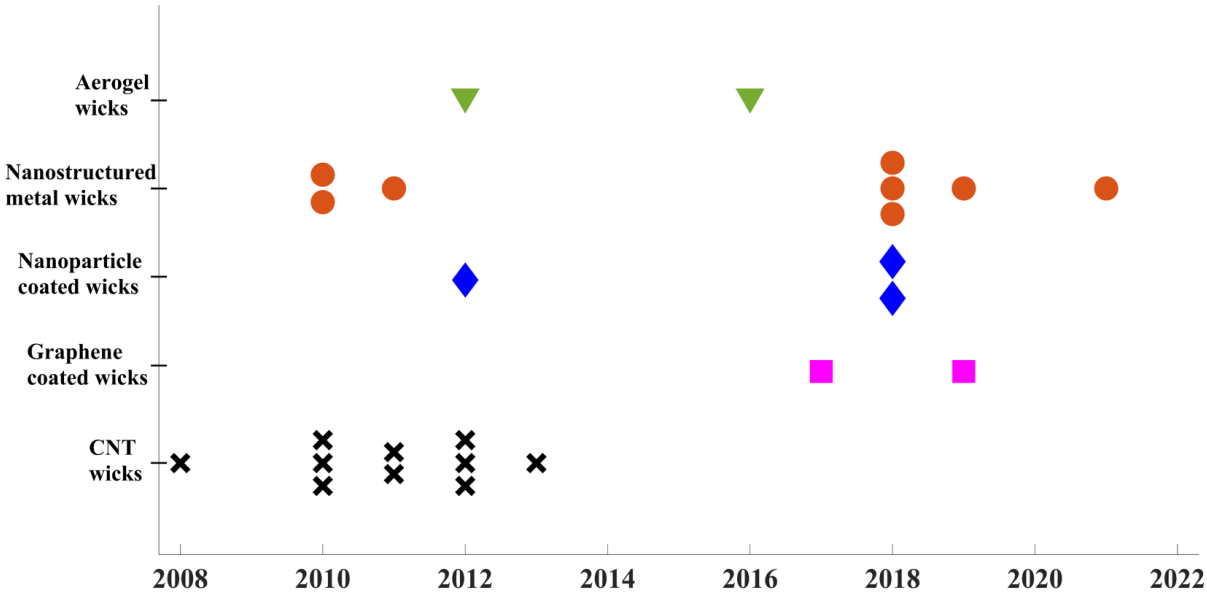

Figure 15: Wick category and publication year of the reviewed papers.

The publication year data shown in figure 15 gives information about the frequency of publications for the different categories of wicks since 2007. It can be seen that nanostructured metal wicks is the category with the most frequent publications and the studies are quite evenly distributed since 2010. Many studies have also been done on carbon nanotube wicks, but those studies are more frequent during the period 2008-2013. The other categories, aerogel wicks, nanoparticle coated wicks and graphene coated wicks are generally not as frequently published. There can be several reasons why some types of wicks are more published than others, e.g. performance, fabrication complexity and cost. Therefore, it was of interest to see if a performance metric could be extracted from the different studies.

A standard characterization test for wick structures is the pool boil experiment. Briefly, the wick to be tested is put on a substrate which in turn is put on a heater with a power input of choice. The wick is partly immersed in a working fluid and the temperature of the substrate is monitored while heating the substrate and wick with a constant heat flux. An efficient wick will provide the hot spot with sufficient working fluid and have an efficient evaporation process to remove the heat. This means that a high-performance wick will contribute to a lower superheat temperature of the substrate compared to a low-performance wick at the same heat flux. Results from pool boil experiments were extracted from the reviewed papers and plotted in the same chart to compare superheat temperatures at different heat fluxes. The plot is shown in figure 16. Before interpreting the results, it is important to know that all data points in figure 16 do not correspond to the critical heat flux of the tested wick. The critical heat flux is the maximum heat flux that the wick can dissipate before experiencing dry-out.

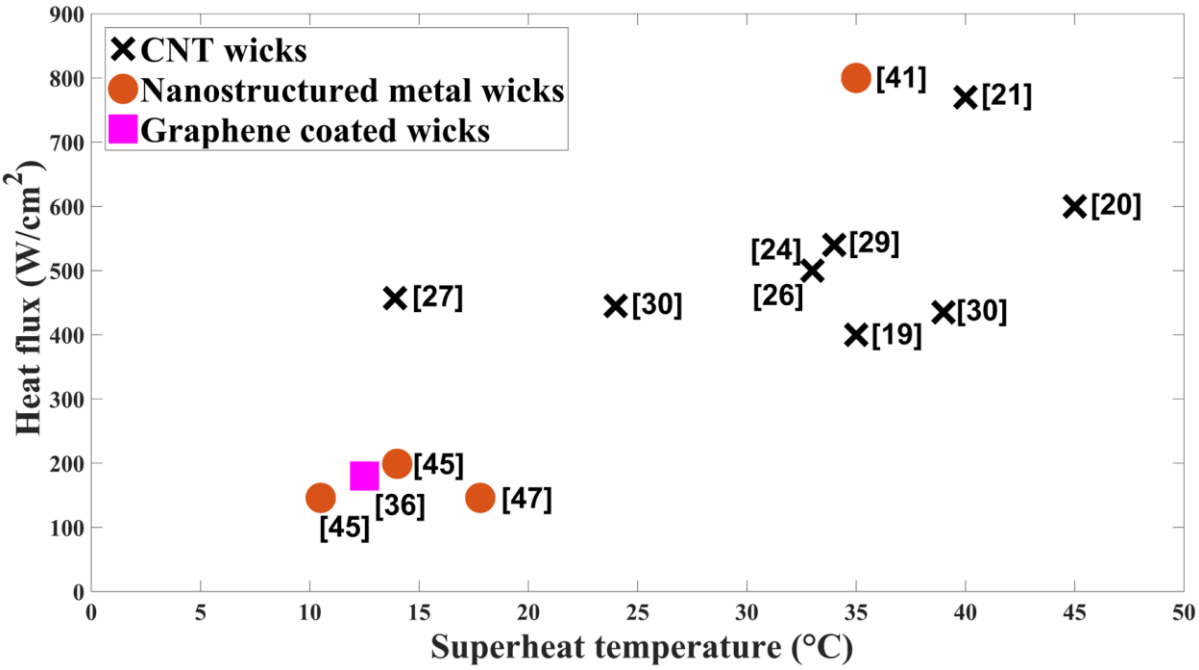

Figure 16: Superheat temperature of the wick substrate during pool boil experiments for some of the reviewed wicks. The numbers in brackets refer to the reference list in paper III.

Figure 16 reveals that carbon nanotube wicks have generally been tested at very high heat fluxes. It can also be seen that the superheat temperatures differ between the various carbon nanotube wicks. However, some of the studies show a very low superheat temperature for high heat flux levels. Despite its good performance at high heat fluxes there have been few papers on carbon nanotube wicks in the last 10 years. At this point it is not completely known why, but likely explanations are simplicity of production and cost. Carbon nanotubes require an expensive chemical vapor deposition tool to be grown and after growth they need to be metal plated or in other ways treated to decrease its hydrophobicity. If similar performance can be obtained with less complicated and cheaper chemical etching procedures, then this is a possible explanation to why carbon nanotube wicks are less frequently studied nowadays.

The data plotted in figure 16 can be used to compare the superheat temperatures for similar heat fluxes. However, it is believed that differences in the used test setups could significantly affect the measured results, hence care must be taken so that the same test procedure has been used to measure the superheat temperature. Instead, it is better to use this model for benchmarking purposes of new wick designs. When a new wick structure is developed, it can be tested with the same method and test setup as one of the studies in figure 16.

4.1.3 Conclusions and outlook

The overall conclusion from the literature study is that nano-enhanced wick structures can significantly improve the performance of vapor chambers and heat pipes. However, there is no definite answer to which the most promising nano-enhanced wick structure for future integration in vapor chambers is. Chemically etched metal structures can have great wettability and thin film area for evaporation and can be processed with straightforward chemical etching processes. Carbon nanotube wicks can achieve high heat fluxes after being patterned and plated with copper to improve their wettability. Other categories of wicks like aerogels, nanoparticle

coatings and graphene coatings have also been shown to be capable but are not as extensively researched.

The most promising wick to integrate in a novel graphene-enhanced vapor chamber will possibly depend on whether it can be grown or attached to graphene-assembled film. Today, few methods exist to reliably attach metals to carbon. Carbon nanotubes, however, can be grown directly on graphene-assembled film. It is deemed a good idea to start with pool boil experiments of several different nano-enhanced wick structures as a pre-study before integrating the wick in prototypes of graphene-enhanced vapor chambers.

4.2 A novel graphene-enhanced vapor chamber

In this section a novel graphene-enhanced vapor chamber concept is presented. Prototypes of the graphene-enhanced vapor chambers were built with lightweight and highly thermally conductive graphene-assembled film as envelope material. Characterization of the prototype vapor chambers was carried out in a customized test setup for measuring thermal resistance of vapor chambers and heat spreaders. The graphene-enhanced vapor chambers were also compared against a commercially available copper vapor chamber in terms of mass-based thermal resistance to show their effective heat dissipating ability per unit mass.

4.2.1 Method

Each prototype vapor chamber was built by using two individual pieces of graphene-assembled film as encapsulating material. A very fine copper mesh was put in between the graphene-assembled films to be used as a wick and the copper mesh was upheld by copper spheres which were soldered in between the copper meshes to act as structural support. The graphene-assembled films were in the end soldered together with a special solder for carbon-based materials with the tradename C-solder from Goodfellow Cambridge Ltd. The different assembly stages of a graphene-enhanced vapor chamber are illustrated in figure 17.

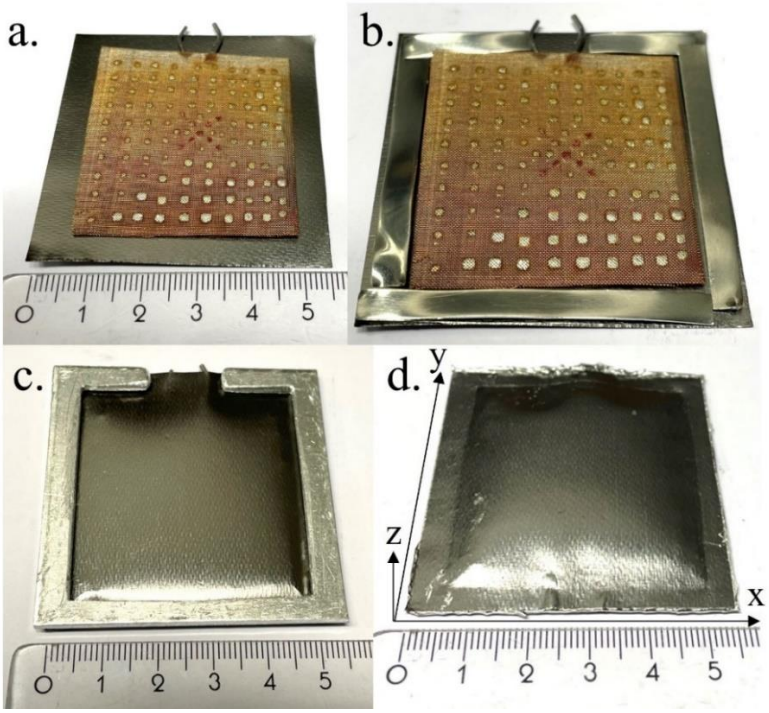

Figure 17: The assembly stages of a graphene-enhanced vapor chamber. a) Two sheets of copper mesh soldered together with copper spheres in between. The copper mesh was put on top of a graphene-assembled film. b) C-solder has been put on the perimeter of the graphene-assembled film. c) An aluminum frame was used to put pressure while reflowing the solder. d) Final graphene-enhanced vapor chamber.

Three different configurations of vapor chambers were fabricated with varying thickness of the graphene-assembled films and spacer diameters. The different configurations are listed in table 2.

Table 2: Graphene-enhanced vapor chamber variants built in this study.

	Graphene-assembled film (µm)	**Spacer diameter (mm)**	**Total VC thickness (mm)**
VC 1	100	2.0	2.7
VC 2	200	1.0	1.9
VC 3	300	1.0	2.1

Figure 17(a-b) shows that two nozzles are inserted into the vapor chamber cavity. The purpose is to be able to fill the vapor chamber with working fluid while venting. Ethanol was the working fluid of choice due to the good wetting properties that was previously illustrated in figure 7. The hydrophobic properties of graphene-assembled film make it unsuitable to use water. The finalized vapor chambers were filled with 0.50 ml of ethanol and sealed with a hot melt adhesive. The vapor chambers were weighed after sealing and before thermal characterization to see if the soldering and hot melt adhesive provided a sufficiently reliable seal. A test setup was built to characterize the performance of the prototype vapor chambers.

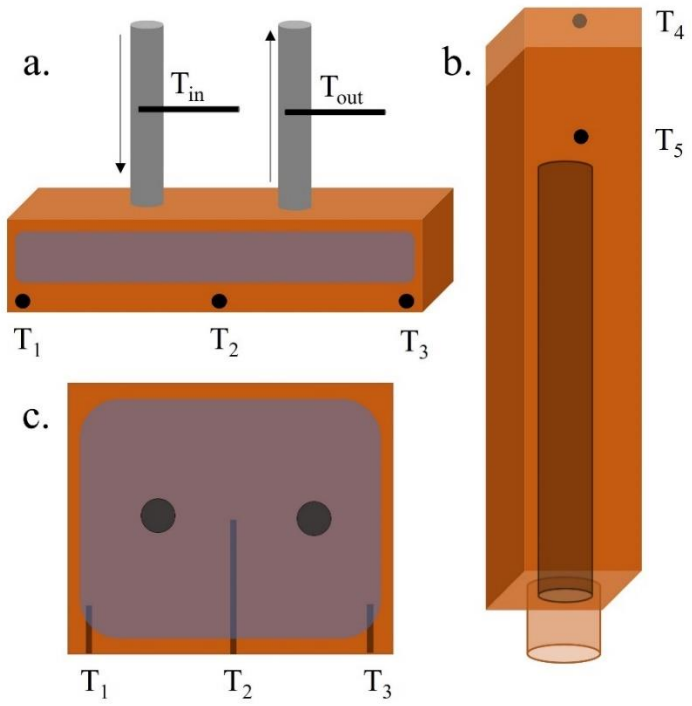

Figure 18: Schematic of thermal test rig for vapor chamber characterization showing placement of temperature sensors. a) Side view of the water-cooled heat sink. b) Copper bar used as hot spot. The center of the copper bar has a reamed hole for a cartridge heater. c) Top view of the water-cooled heat sink.

The vapor chamber test rig consists of an 8x8 mm^2 hot spot which is placed in the center of the bottom side of the vapor chamber and a water-cooled heat sink on the other side. The heat is provided by a 30 W cartridge heater which is inserted into the copper bar. The vapor chamber is clamped between the heater bar and the heat sink by applying compression force with a torque controlled M10 screw. The heater and heat sink were built so that it can operate inside a vacuum chamber, this enables measurements in low pressure if desirable. The locations of the temperature sensors are carefully selected to be able to monitor the heat spreading properties of the vapor chambers in the x-y plane as well as in the z-direction. The thermal test rig can be seen in figure 19.

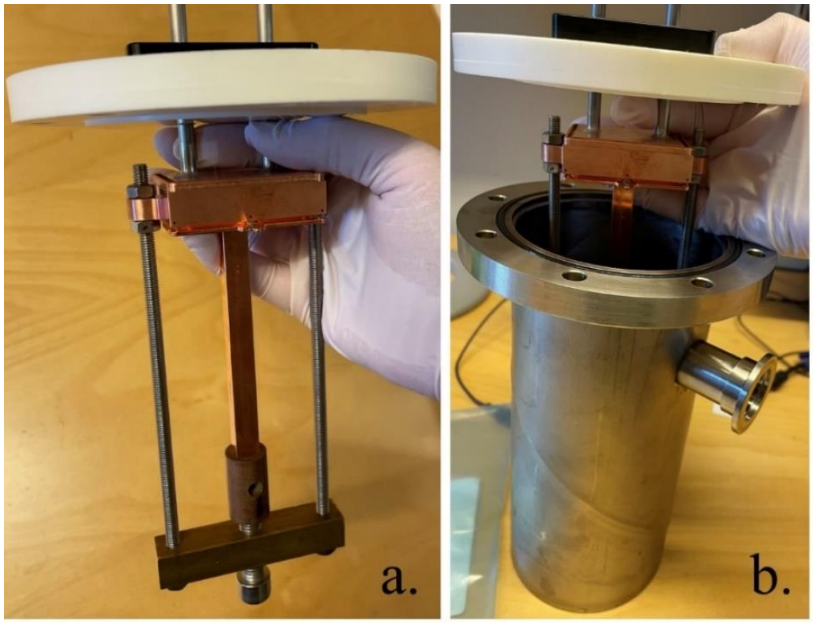

Figure 19: Thermal test rig for vapor chamber characterization. a) Heater and heat sink with a frame that enables torque control of assembly pressure of the tested vapor chamber. b) Heater and heat sink operate inside a steel container.

The vapor chamber measurements were run for 330 seconds. This test time gave enough time to be able to make the temperatures in the system reach steady state for most of the tested vapor chambers. The temperatures measured during the tests were used to calculate the thermal resistance of the vapor chambers. To account for the heat spreading properties of the vapor chambers a thermal resistance parameter was calculated which accounted for T_1, T_2 and T_3 in the heat sink, as well as the hot spot temperature T_4 as outlined in figure 18. The following equation was used to calculate the total thermal resistance:

$$R_{Tot} = \frac{A * (T_4 - \frac{T_1 + T_2 + T_3}{3})}{P} \tag{7}$$

Furthermore, the mass of the individual vapor chambers was accounted for by introducing a new mass-based figure of merit by multiplying R_{Tot} with the mass, m_{VC}, of the tested vapor chamber:

$$R_{Tot_{mass}} = R_{Tot} * m_{VC} \tag{8}$$

Figure 18 also shows that the cooling water temperature is measured on the inlet and outlet. By knowing the temperature difference of the cooling-water it is possible to calculate how much heat that has been transferred to the heat sink and how much heat that has been lost to the ambient air via convection and radiation. This is done by taking the product of the density of the cooling water, volume flow rate, the specific heat capacity of the cooling water and the temperature difference between the inlet and outlet of the cooling water:

$$Q = \rho_{water} \dot{V} c_p (T_{out} - T_{in}) \tag{9}$$

4.2.2 Results and discussion

The three prototype vapor chambers outlined in table 2 were characterized in the thermal test rig which can be seen in figure 19. One of the vapor chambers, VC 2, was also measured empty to see the effect of working fluid. The best performing prototype graphene-enhanced vapor chamber, VC 3, was compared against a solid copper block and a commercial copper vapor chamber. The results from the characterization are shown in figure 20 where the total thermal resistance and mass-based thermal resistance has been calculated from equation 7 and 8 and plotted against measurement time.

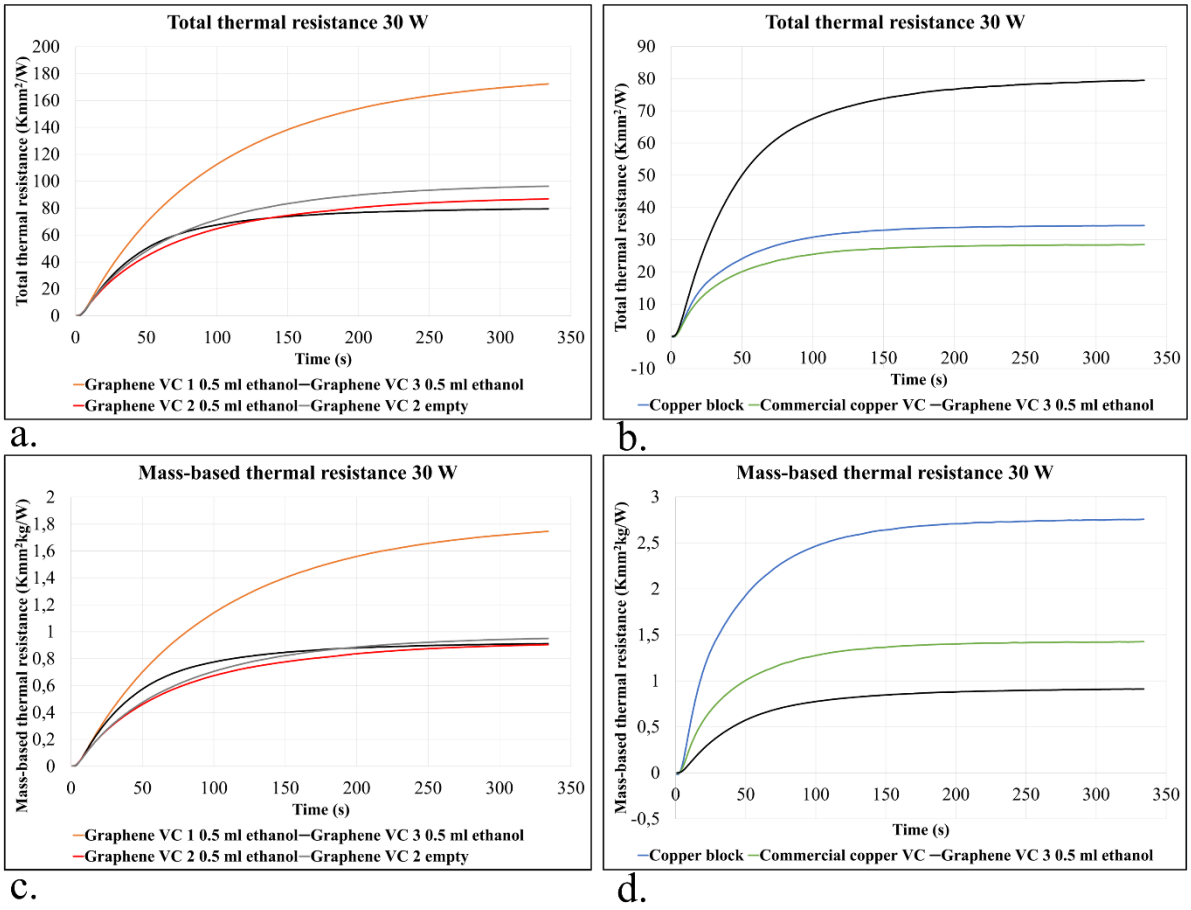

Figure 20: Total thermal resistance and mass-based thermal resistance as function of measurement time. a) Total thermal resistance of the prototype graphene-enhanced vapor chambers. b) Total thermal resistance of VC 3 compared to a solid copper block and a commercial copper vapor chamber. c) Mass-based thermal resistance of the prototype graphene-enhanced vapor chambers. d) Mass-based thermal resistance of VC 3 compared to a solid copper block and a commercial copper vapor chamber.

In figure 20(a) it can be seen that VC 1 has the highest thermal resistance of the tested design configurations. The observed difference is believed to be mainly due to that VC 1 has a larger spacer thickness compared to VC 2 and 3. The prototype vapor chamber with the lowest thermal resistance is VC 3, it performs slightly better than VC 2. The main difference between the two is that a 300 µm thick graphene-assembled film was used to build VC 3 and a 200 µm thick film was used in VC 2. The empty VC 2 performs slightly worse than both VC 2 with 0.50 ml working fluid and VC 3. The positive effect of the working fluid is noticeable but not as great as one might have expected. This means that the thermal conductivity in the cavity of

the vapor chamber is not optimal and further improvement work can be done to optimize the two-phase cooling process. It is also believed that the difference in thermal resistance between VC 1 and the other prototypes would have been smaller if the two-phase heat transfer had worked better.

Another thing that could have affected the results is leak tightness. The prototype vapor chambers were weighed before and after characterization, the results are presented in table 3.

Table 3: Mass of two of the fabricated graphene-enhanced vapor chambers before and after characterization.

	Mass before measurement (g)	**Mass after measurement (g)**	**Volume filled (ml)**	**Volume lost (ml)**
VC 2	10.41	10.19	0.50	0.28
VC 3	11.47	11.37	0.50	0.13

Table 3 shows that both VC 2 and 3 had issues with leak tightness during the measurement. A high mounting pressure and elevated temperature resulted in a pressure rise in the chamber that could cause delamination of the graphene-assembled films and create leak paths. When comparing VC 2 and 3 in terms of leak tightness it can be seen that VC 3 lost less working fluid during operation. The difference in leak tightness is a possible explanation to why VC 3 performs slightly better than VC 2 in terms of total thermal resistance.

In figure 20(b) the performance of VC 3 is compared to a solid copper block and a commercial copper vapor chamber. In terms of total thermal resistance, the performance of the graphene-enhanced prototype is at this point not as low as the already commercially available alternatives. It is, however, worth mentioning that a hand-made prototype of a new concept with lower technology readiness level (TRL) is being compared to one of the most effective passive cooling devices on the market. At this point it cannot be expected that the graphene-enhanced vapor chamber should be able to compete with the commercially available alternatives.

One of the major advantages of graphene-assembled film, except for thermal conductivity, is its low density which contributes to a very low mass of the prototype devices. Figure 20(d) shows the comparison of mass-based thermal resistance, $R_{Tot_{mass}}$, between VC 3, a copper block, and the commercial copper vapor chamber. When mass is accounted for in the thermal resistance parameter, VC 3 clearly outperforms the commercial alternative. This result implies that, if the sealing issue is solved, the graphene-enhanced vapor chambers can have great potential in lightweight electronics applications.

The individual readings from each temperature sensor can be further analyzed to better understand how the vapor chambers perform. Table 4 shows the temperature rise of each individual temperature sensor during the steady state measurements. It also shows the measured temperature rise of the cooling water and how much energy that was transferred to the cooling water during the measurement as calculated by equation 9.

Table 4: Temperature rise of each individual temperature sensor, increase in cooling-water temperature and energy transfer to the cooling-water during the steady state measurements.

	ΔT_1 (°C)	ΔT_2 (°C)	ΔT_3 (°C)	ΔT_4 (°C)	ΔT cooling water (°C)	Q (W)
Copper block	1.09	1.85	1.67	17.75	0.41	28.5
Commercial copper VC	1.06	1.87	1.71	14.93	0.39	27.1
Graphene VC 3 0.5 ml ethanol	1.12	1.72	1.51	38.66	0.36	25.0

Table 4 reveals that the temperature increase of the hot spot temperature, ΔT_4, is the highest for VC 3 and lowest for the commercial VC. This result is in line with the total thermal resistance that was shown in figure 20(b). A higher thermal resistance and hot spot temperature also means that the heat transfer to the cooling-water is lower. In total 25 W out of the initial power input of 30 W is calculated to be transferred away with the cooling-water for VC 3. A higher thermal resistance means that more heat will be transferred away with other heat transfer mechanisms. In this case it means that 5 W is transferred to the inside of the steel vessel via convection and radiation and thereby heating up the air inside. It is believed that the heat losses to the steel vessel is the reason why the vapor chambers with high thermal resistance in general did not reach steady state during the measurements.

Another interesting observation from table 4 is the readings from ΔT_1 and ΔT_2. The temperature increase at T_1 is highest for VC 3 and the increase at T_2 is highest for the commercial VC. The temperature sensor T_1 is located closest to the cooling water inlet, hence, a comparatively higher temperature rise at T_1 means better heat spreading. T_2 is located directly above the hot spot which means that a higher ΔT_2 means better heat transfer in z-direction. These results imply that the graphene-enhanced vapor chamber has better heat spreading properties and worse heat transfer in z-direction compared to the commercial copper VC. The anisotropic heat transfer can be derived from the graphene-assembled film. As discussed in chapter 2, the graphene-assembled film consists of a layered structure of graphene with the flakes aligned in the x-y plane. With the current material choices, it can be argued that the graphene-enhanced vapor chamber would be more competitive if it is as large as possible in the x-y plane and as thin as possible in z-direction.

4.2.3 Conclusions and outlook

Graphene-assembled film can be used to build vapor chambers with a mass-based thermal resistance that is 36% lower than a commercial copper vapor chamber. This is promising for future lightweight electronics applications with high performance cooling requirements. However, at this early point in the development stage the commercial copper vapor chamber still has a lower total thermal resistance. Several design changes should be addressed to improve the graphene-enhanced vapor chamber performance and its TRL before it can be applied in real electronics applications. The sealing issue needs to be addressed both to improve performance but also to create a reliable device that does not risk damaging surrounding electronic devices when put into an application. This challenge should be addressed in coming

studies. Furthermore, graphene-assembled films currently prevent usage of water as working fluid. The wettability properties of the graphene-assembled film are not suitable for water, but the wettability can be modified. Different wettability modification processes and the effects on performance of a graphene-enhanced vapor chamber should be studied. Lastly, it is believed that the performance of the graphene-enhanced vapor chamber can be significantly improved by enhancing the liquid transport properties of the wick. A standard copper mesh was used in this study, but this can be changed to a high-performance nano-enhanced wick from one of the categories reviewed in paper III.

5. General conclusions and outlook

Graphene-based thermal management products are gaining popularity on the market due to the suitable properties of graphene. However, graphene-based products in thermal management applications are still novel and more knowledge about reliability and production processes can expand application areas and speed up commercialization.

In this thesis, the production process of a graphene-assembled film heat spreader was evaluated to achieve a higher thermal conductivity. Additionally, a vertically aligned graphene-based TIM was evaluated in terms of reliability in three different reliability tests. Furthermore, nano enhanced vapor chambers were studied. First, the best options for future integration of nano-enhanced wick structures in vapor chambers were assessed in a literature study and then graphene-assembled film was evaluated to be used as encapsulating material in a novel graphene-enhanced vapor chamber.

The performance of a graphene-assembled film was evaluated after extending the high temperature annealing time in the production process. Defect and oxygen free graphene with large grain size could be achieved by annealing the self-assembled GO in a two-phase process at a maximum of 2850°C for up to four hours. The thermal conductivity was characterized by the Joule heating method and the long annealing time resulted in a thermal conductivity of 3826 W/mK for the 1 μm thick film. The effect that the thermal annealing process has on a real thermal management application was demonstrated by comparing an annealed film with a non-annealed GO film. The hot spot temperature of a high-power LED was seen to be 47 degrees lower after annealing the GO film.

A test method was developed to evaluate the thermal resistance of the vertically aligned graphene-based TIMs over time. The test method was deemed to be successful and enabled continuous monitoring of thermal resistance while maintaining a constant compression of the TIM. In general, the measured thermal resistance showed little degradation over time with small differences observed between the different reliability tests. The vertically aligned graphene-based TIM was shown to have a very stable performance over time when subjected to thermal aging, thermal cycling, and damp heat tests. The high resistance to aging, dry-out and moisture paves way for this type of TIM to be used in applications which require high performance without the need to periodically change the TIM.

The most promising nano-enhanced wick structures that have been researched since 2008 were reviewed in a literature study. The idea was to get knowledge about what type of wick structure that should be integrated into novel vapor chambers to further improve their performance. Generally, it was concluded that nano wick structures can significantly improve the performance of vapor chambers. However, there was no unambiguous answer to which one is the best. The two most studied categories of wicks were carbon nanotube and nanostructured metal wicks. With carbon nanotube wicks, one can achieve high heat fluxes in pool boil experiments, and they can be grown directly on the graphene-assembled film. The nanostructured metal wicks show that super hydrophilicity and a large thin film area for evaporation can be achieved with relatively simple chemical etching processes. Several wick alternatives should be evaluated separately in pool boiling experiments before integration into the graphene-enhanced vapor chamber.

Moreover, graphene-assembled film was used to build lightweight and high-performance graphene-enhanced vapor chambers. This new concept of using graphene-assembled film as encapsulating material in a vapor chamber was shown to significantly reduce the weight of the device compared to a commercial copper vapor chamber of equal size. The mass-based thermal resistance of the best performing prototype graphene-enhanced vapor chamber was 36% lower compared to that of the commercial copper vapor chamber used for benchmarking. The graphene-enhanced vapor chamber concept is believed to have great potential in lightweight cooling applications if three design issues can be solved in future work. These design issues are leak tightness, water wettability and wick structure.

This thesis has revealed some new knowledge about the reliability and performance of graphene-based heat spreaders and TIMs and how they can be advantageous to use instead of more conventional metal-based materials in thermal management solutions. The new graphene-enhanced vapor chamber also demonstrates that new applications can be found and improved with graphene-based materials. This can potentially help increase the market share of graphene-based products in electronics cooling applications in the future. Having more graphene-based products in electronics cooling would not only be advantageous for the graphene industry, but it can also help to build lightweight, reliable, sustainable, and efficient thermal management solutions.

Acknowledgements

Many people have contributed to the work that resulted in this thesis, for this, they deserve my recognition and genuine gratitude. First, my supervisor and examiner Professor Johan Liu, thank you for continuous supervision and the opportunity to conduct research on this inspiring and important research topic. My co-supervisors Dr. Torbjörn Nilsson and Docent Yifeng Fu, thank you for contributing with your expertise, research guidance and for giving me valuable feedback on my writing. The work in this thesis was funded by 2D TECH VINNNOVA competence center (Ref. 2019-00068).

I want to express my gratitude to my friends and colleagues at the Electronics Packaging and MEMS group who have in various ways helped me and made this work very enjoyable over the years: Per Lundgren, Sadia Farjana, Azega Rajendra Babu Kalai Arasi, Mazharul Haque, Muhammad Hassan, Hafid Zehri, Sihua Guo, Athanasios Theodoridis and Oscar Nordin. Furthermore, I want to express my appreciation to all colleagues in the Electronics Materials and Systems Laboratory (EMSL) for creating such a friendly and welcoming workplace. A special thanks to my friend and former colleague Andreas Nylander for always taking his time to help me and give me valuable advice when first coming to EMSL.

I would also like to thank Lars Jönsson from the Department of Microtechnology and Nanoscience (MC2) for his work with building test rigs that were used for characterization of TIMs and vapor chambers. Furthermore, I would also like to acknowledge the Nanofabrication Laboratory (NFL) and its staff for providing helpful knowledge and training on fabrication and analysis tools in the MC2 cleanroom.

Thanks also to the people I have collaborated with from industry. Dr. Kai Kallio and Arian Kamal at the Material Centre at Volvo Car Corporation, for your valuable advice, material analysis expertise and help with building a test setup for thermal characterization. Dr. Murali Murugesan, Amos Nkansah and Hongfeng Zhang from SHT Smart High-Tech AB for manufacturing and providing graphene-assembled film and vertically aligned graphene TIMs for the studies in this thesis.

This thesis was also made possible by the endless support and encouragement from my family; my mother Susanne, my father Roger and brother Mattias. Finally, my partner and love Karolina who has supported me through many late hours in the laboratory and long writing sessions, thank you for all your support and understanding.

Markus Enmark
Göteborg, February 2024

References

[1] A. L. Moore and L. Shi, "Emerging challenges and materials for thermal management of electronics," *Mater. Today*, vol. 17, no. 4, pp. 163–174, May 2014, doi: 10.1016/J.MATTOD.2014.04.003.

[2] Y. Fu, J. Hansson, Y. Liu, S. Chen, A. Zehri, M. Kabiri Samani, N. Wang, Y. Ni, Y. Zhang, Z.-B. Zhang, Q. Wang, M. Li, H. Lu, M. Sledzinska, C. M. Sotomayor Torres, S. Volz, A. A. Balandin, X. Xu, and J. Liu, "Graphene related materials for thermal management," *2D Mater.*, vol. 7, no. 1, p. 012001, 2020, doi: 10.1088/2053-1583/ab48d9.

[3] A.Theodoridis, "Characterization of graphene based porous structures for noise damping in transmission systems," Chalmers University of Technology, 2022.

[4] F. G. Torres, O. P. Troncoso, L. Rodriguez, and G. E. De-La-Torre, "Sustainable synthesis, reduction and applications of graphene obtained from renewable resources," *Sustain. Mater. Technol.*, vol. 29, no. e00310, 2021, doi: 10.1016/j.susmat.2021.e00310.

[5] K. S. Novoselov, A. K. Geim, S. V. Morozov, D. Jiang, Y. Zhang, S. V. Dubonos, I. V. Grigorieva, and A. A. Firsov, "Electric field in atomically thin carbon films," *Science*, vol. 306, no. 5696, pp. 666–669, Oct. 2004, doi: 10.1126/SCIENCE.1102896.

[6] A. K. Geim and K. S. Novoselov, "The rise of graphene," *Nat. Mater.*, vol. 6, no. 3, pp. 183–191, 2007.

[7] "ISO80004-1:2023 Nanotechnologies - Vocabulary - Part 1: Core vocabulary." [Online]. Available: https://www.iso.org/standard/79525.html

[8] Sigma Aldrich, "Carbon Nanomaterials." [Online]. Available: https://www.sigmaaldrich.com/SE/en/products/materials-science/electronic-materials/carbon-nanomaterials

[9] C. Lee, X. Wei, J. W. Kysar, and J. Hone, "Measurement of the elastic properties and intrinsic strength of monolayer graphene," *Science*, vol. 321, no. 5887, pp. 385–388, Jul. 2008, doi: 10.1126/SCIENCE.1157996.

[10] S. Stankovich, D. A. Dikin, G. H. B. Dommett, K. M. Kohlhaas, E. J. Zimney, E. A. Stach, R. D. Piner, S. T. Nguyen, and R. S. Ruoff, "Graphene-based composite materials," *Nature*, vol. 442, no. 20, 2006, doi: 10.1038/nature04969.

[11] X. Wang and G. Shi, "Flexible graphene devices related to energy conversion and storage," *Energy Environ. Sci.*, vol. 8, no. 3, pp. 790–823, 2015, doi: 10.1039/c4ee03685a.

[12] H. Shen, L. Zhang, M. Liu, and Z. Zhang, "Biomedical Applications of Graphene," *Theranostics*, vol. 2012, no. 3, pp. 283–294, 2012, doi: 10.7150/thno.3642.

[13] X. Li, G. Zhang, X. Bai, X. Sun, X. Wang, E. Wang, and H. Dai, "Highly conducting graphene sheets and Langmuir-Blodgett films," *Nat. Nanotechnol.*, vol. 3, no. 9, pp. 538–542, 2008, doi: 10.1038/nnano.2008.210.

[14] M. Sang, J. Shin, K. Kim, and K. J. Yu, "Electronic and Thermal Properties of Graphene and Recent Advances in Graphene Based Electronics Applications,"

Nanomaterials, vol. 9, no. 3, p. 374, 2019, doi: 10.3390/nano9030374.

[15] T. S. Sreeprasad and V. Berry, "How Do the Electrical Properties of Graphene Change with its Functionalization?," *Small*, vol. 9, no. 3, pp. 341–350, 2013, doi: 10.1002/smll.201202196.

[16] L. Chen, N. Li, X. Yu, S. Zhang, C. Liu, Y. Song, Z. Li, S. Han, W. Wang, P. Yang, N. Hong, S. Ali, and Z. Wang, "A general way to manipulate electrical conductivity of graphene," *Chem. Eng. J.*, vol. 462, p. 142139, Apr. 2023, doi: 10.1016/J.CEJ.2023.142139.

[17] A. Nylander, "Fundamental Characterization of Low Dimensional Carbon Nanomaterials for 3D Electronics Packaging," Chalmers University of Technology, 2021.

[18] A. A. Balandin, "Thermal properties of graphene and nanostructured carbon materials," *Nat. Mater.*, vol. 10, no. 8, pp. 569–581, 2011, doi: 10.1038/NMAT3064.

[19] W. S. Hummers and R. E. Offeman, "Preparation of Graphitic Oxide," 1958, Accessed: Dec. 01, 2023. [Online]. Available: https://pubs.acs.org/sharingguidelines

[20] D. A. Dikin, S. Stankovich, E. J. Zimney, R. D. Piner, G. H. B. Dommett, G. Evmenenko, S. T. Nguyen, and R. S. Ruoff, "Preparation and characterization of graphene oxide paper," *Nature*, vol. 448, no. 7152, pp. 457–460, 2007, doi: 10.1038/nature06016.

[21] J. Xiang and L. T. Drzal, "Thermal conductivity of exfoliated graphite nanoplatelet paper," *Carbon*, vol. 49, no. 3, pp. 773–778, 2011, doi: 10.1016/j.carbon.2010.10.003.

[22] G. Xin, H. Sun, T. Hu, R. Fard, X. Sun, N. Koratkar, T. Borca-Tasciuc, J. Lian, and J. Lian, "Large-Area Freestanding Graphene Paper for Superior Thermal Management," *Adv. Mater*, vol. 26, pp. 4521–4526, 2014, doi: 10.1002/adma.201400951.

[23] N.-J. Song, C.-M. Chen, C. Lu, Z. Liu, Q.-Q. Kong, and R. Cai, "Thermally reduced graphene oxide films as flexible lateral heat spreaders," *J. Mater. Chem. A*, vol. 2, no. 39, pp. 16563–16568, 2014, doi: 10.1039/c4ta02693d.

[24] N. Wang, M. Kabiri Samani, H. Li, L. Dong, Z. Zhang, P. Su, S. Chen, J. Chen, S. Huang, G. Yuan, X. Xu, B. Li, K. Leifer, L. Ye, J. Liu, N. Wang, M. K. Samani, P. Su, J. Liu, H. Li, K. Leifer, L. Dong, Z. Zhang, J. Chen, X. Xu, S. Chen, S. Huang, G. Yuan, B. Li, and L. Ye, "Tailoring the Thermal and Mechanical Properties of Graphene Film by Structural Engineering," *Small*, vol. 14, no. 29, p. 1801346, 2018, doi: 10.1002/smll.201801346.

[25] B. Shen, W. Zhai, and W. Zheng, "Ultrathin Flexible Graphene Film: An Excellent Thermal Conducting Material with Efficient EMI Shielding," *Adv. Funct. Mater.*, vol. 24, no. 28, pp. 4542–4548, Jul. 2014, doi: 10.1002/ADFM.201400079.

[26] S. Chen, Q. Wang, M. Zhang, R. Huang, Y. Huang, J. Tang, and J. Liu, "Scalable production of thick graphene films for next generation thermal management applications," *Carbon*, vol. 167, no. 15, pp. 270–277, 2020, doi: 10.1016/j.carbon.2020.06.030.

[27] "SHT Smart High-Tech AB." [Online]. Available: https://smarthightech.com/

[28] J. Hansson, T. M. J. Nilsson, L. Ye, and J. Liu, "Novel nanostructured thermal

interface materials: A review," *Int. Mater. Rev.*, vol. 63, no. 1, pp. 22–45, 2018, doi: 10.1080/09506608.2017.1301014.

[29] B. P. Grady, *Carbon Nanotube-Polymer Composites: Manufacture, Properties, and Applications.* John Wiley & Sons, Inc, 2011.

[30] Z. Han and A. Fina, "Thermal conductivity of carbon nanotubes and their polymer nanocomposites: A review," *Prog. Polym. Sci.*, vol. 36, pp. 914–944, 2011, doi: 10.1016/j.progpolymsci.2010.11.004.

[31] W.-L. Song, W. Wang, L. M. Veca, C. Y. Kong, M.-S. Cao, P. Wang, M. J. Meziani, H. Qian, G. E. Lecroy, L. Cao, and Y.-P. Sun, "Polymer/carbon nanocomposites for enhanced thermal transport properties-carbon nanotubes versus graphene sheets as nanoscale fillers," *J. Mater. Chem.*, vol. 22, pp. 17133–17139, 2012, doi: 10.1039/c2jm32469e.

[32] S. Xu and J. Zhang, "Vertically Aligned Graphene for Thermal Interface Materials," *Small Struct.*, vol. 1, no. 3, p. 2000034, 2020, doi: 10.1002/sstr.202000034.

[33] N. Wang, Y. Liu, S. Chen, L. Ye, and J. Liu, "Highly Thermal Conductive and Electrically Insulated Graphene Based Thermal Interface Material with Long-term Reliability," *2019 IEEE 69th Electron. Components Technol. Conf.*, pp. 1564–1568, 2019, doi: 10.1109/ECTC.2019.00240.

[34] M. Bulut, S. G. Kandlikar, and N. Sozbir, "A Review of Vapor Chambers," *Heat Transf. Eng.*, vol. 40, no. 19, pp. 1551–1573, Nov. 2019, doi: 10.1080/01457632.2018.1480868.

[35] R. B. Ganvir, P. V Walke, and V. M. Kriplani, "Heat transfer characteristics in nanofluid-A review," *Renew. Sustain. Energy Rev.*, vol. 75, pp. 451–460, 2017, doi: 10.1016/j.rser.2016.11.010.

[36] C. Y. Tsai, H. T. Chien, P. P. Ding, B. Chan, T. Y. Luh, and P. H. Chen, "Effect of structural character of gold nanoparticles in nanofluid on heat pipe thermal performance," *Mater. Lett.*, vol. 58, no. 9, pp. 1461–1465, 2004, doi: 10.1016/j.matlet.2003.10.009.

[37] S.-W. Kang, W.-C. Wei, S.-H. Tsai, and S.-Y. Yang, "Experimental investigation of silver nano-fluid on heat pipe thermal performance," *Appl. Therm. Eng.*, vol. 26, no. 17–18, pp. 2377–2382, 2006, doi: 10.1016/j.applthermaleng.2006.02.020.

[38] M. Alhuyi Nazari, R. Ghasempour, M. Hossein Ahmadi, G. Heydarian, and M. Behshad Shafii, "Experimental investigation of graphene oxide nanofluid on heat transfer enhancement of pulsating heat pipe," *Int. Commun. Heat Mass Transf.*, vol. 91, pp. 90–94, 2018, doi: 10.1016/j.icheatmasstransfer.2017.12.006.

[39] N. Putra, W. N. Septiadi, R. Sahmura, and C. T. Anggara, "Application of Al2O3 Nanofluid on Sintered Copper-powder Vapor Chamber for Electronic Cooling," *Adv. Mater. Res.*, vol. 789, pp. 423–428, 2013, doi: 10.4028/www.scientific.net/AMR.789.423.

[40] N. K. Gupta, A. K. Tiwari, and S. K. Ghosh, "Experimental Study of Thermal Performance of Nanofluid-Filled and Nanoparticles-Coated Mesh Wick Heat Pipes," *J. Heat Transfer*, vol. 140, no. 10, Oct. 2018, doi: 10.1115/1.4040146/374541.

[41] H. Seok Jo, S. An, X. Hung Nguyen, Y. Il Kim, B.-H. Bang, S. C. James, J. Choi, and

S. S. Yoon, “Modifying capillary pressure and boiling regime of micro-porous wicks textured with graphene oxide,” *Appl. Therm. Eng.*, vol. 128, pp. 1605–1610, 2018, doi: 10.1016/j.applthermaleng.2017.09.103.

[42] M. Mehrali, E. Sadeghinezhad, S. T. Latibari, S. N. Kazi, M. Mehrali, M. N. Bin, M. Zubir, H. Simon, and C. Metselaar, “Investigation of thermal conductivity and rheological properties of nanofluids containing graphene nanoplatelets,” *Nanoscale Res. Lett.*, vol. 9, no. 15, pp. 1–12, 2014.

[43] E. Sadeghinezhad, M. Mehrali, M. A. Rosen, A. Reza Akhiani, S. Tahan Latibari, M. Mehrali, and H. Simon Cornelis Metselaar, “Experimental investigation of the effect of graphene nanofluids on heat pipe thermal performance,” *Appl. Therm. Eng.*, vol. 100, pp. 775–787, 2016, doi: 10.1016/j.applthermaleng.2016.02.071.

[44] Y. Liu, S. Chen, Y. Fu, N. Wang, D. Mencarelli, L. Pierantoni, H. Lu, and J. Liu, “A lightweight and high thermal performance graphene heat pipe,” *Nano Sel.*, vol. 2, no. 2, pp. 364–372, Feb. 2021, doi: 10.1002/NANO.202000195.

[45] L. Zhang, G. Zhang, C. Liu, and S. Fan, “High-Density Carbon Nanotube Buckypapers with Superior Transport and Mechanical Properties,” *Nano Lett*, vol. 12, p. 51, 2012, doi: 10.1021/nl3023274.

[46] E. Pop, D. Mann, Q. Wang, K. Goodson, and H. Dai, “Thermal Conductance of an Individual Single-Wall Carbon Nanotube above Room Temperature,” *Nano Lett.*, vol. 6, no. 1, pp. 96–100, 2006, doi: 10.1021/nl052145f.

[47] G. Q. Zhang, J. P. Zheng, R. Liang, A. -, W. Zhu, C. Zeng, J. P. Zheng, D. Wang, P. Song, C. Liu, W. Wu, and S. Fan, “Highly oriented carbon nanotube papers made of aligned carbon nanotubes,” *Nanotechnology*, vol. 19, p. 6, 2008, doi: 10.1088/0957-4484/19/7/075609.

[48] X. Guo, S. Cheng, W. Cai, Y. Zhang, and X. Zhang, “A review of carbon-based thermal interface materials: Mechanism, thermal measurements and thermal properties,” *Mater. Des.*, vol. 209, p. 109936, 2021, doi: 10.1016/j.matdes.2021.109936.

[49] J. A. Weibel, S. V Garimella, J. Y. Murthy, and D. H. Altman, “Design of Integrated Nanostructured Wicks for High-Performance Vapor Chambers,” *IEEE Trans. COMPONENTS, Packag. Manuf. Technol.*, vol. 1, no. 6, 2011, doi: 10.1109/TCPMT.2011.2132721.

[50] A. B. Solomon, K. Ramachandran, and B. C. Pillai, “Thermal performance of a heat pipe with nanoparticles coated wick,” *Appl. Therm. Eng.*, vol. 36, pp. 106–112, 2012, doi: 10.1016/j.applthermaleng.2011.12.004.

[51] Y. Nam, S. Sharratt, C. Byon, S. J. Kim, and Y. S. Ju, “Fabrication and Characterization of the Capillary Performance of Superhydrophilic Cu Micropost Arrays,” *J. Microelectromechanical Syst.*, vol. 19, no. 3, pp. 581–588, 2010, doi: 10.1109/JMEMS.2010.2043922.

[52] A. Faghri, *Heat pipe science and technology*. Taylor & Francis, 1995.

[53] J. Velardo, A. Date, R. Singh, J. Nihill, A. Date, T. L. Phan, and M. Takahashi, “Experimental investigation of a vapour chamber heat spreader with hybrid wick structure,” *Int. J. Therm. Sci.*, vol. 140, pp. 28–35, 2019, doi:

10.1016/j.ijthermalsci.2019.02.009.

[54] T. Semenic and I. Catton, “Experimental study of biporous wicks for high heat flux applications,” *J. Heat Mass Transf.*, vol. 52, no. 21–22, pp. 5113–5121, 2009, doi: 10.1016/j.ijheatmasstransfer.2009.05.005.

[55] Q. Cai and A. Bhunia, “High heat flux phase change on porous carbon nanotube structures,” *Int. J. Heat Mass Transf.*, vol. 55, no. 21–22, pp. 5544–5551, 2012, doi: 10.1016/j.ijheatmasstransfer.2012.05.027.

[56] R. Wen, S. Xu, Y.-C. Lee, and R. Yang, “Capillary-driven liquid film boiling heat transfer on hybrid mesh wicking structures,” *Nano Energy*, vol. 51, pp. 373–382, 2018, doi: 10.1016/j.nanoen.2018.06.063.

[57] S. M. Jung, H. Y. Jung, M. S. Dresselhaus, Y. J. Jung, and J. Kong, “A facile route for 3D aerogels from nanostructured 1D and 2D materials,” *Sci. Rep.*, vol. 2, no. 1, p. 849, 2012, doi: 10.1038/srep00849.